PIP$_2$ depletion promotes TRPV4 channel activity in mouse brain capillary endothelial cells

Osama F Harraz[1], Thomas A Longden[1], David Hill-Eubanks[1], Mark T Nelson[1,2]*

[1]Department of Pharmacology, University of Vermont, Burlington, United States; [2]Institute of Cardiovascular Sciences, Manchester, United Kingdom

Abstract We recently reported that the inward-rectifier Kir2.1 channel in brain capillary endothelial cells (cECs) plays a major role in neurovascular coupling (NVC) by mediating a neuronal activity-dependent, propagating vasodilatory (hyperpolarizing) signal. We further demonstrated that Kir2.1 activity is suppressed by depletion of plasma membrane phosphatidylinositol 4,5-bisphosphate (PIP$_2$). Whether cECs express depolarizing channels that intersect with Kir2.1-mediated signaling remains unknown. Here, we report that Ca^{2+}/Na$^+$-permeable TRPV4 (transient receptor potential vanilloid 4) channels are expressed in cECs and are tonically inhibited by PIP$_2$. We further demonstrate that depletion of PIP$_2$ by agonists, including putative NVC mediators, that promote PIP$_2$ hydrolysis by signaling through G$_q$-protein-coupled receptors (G$_q$PCRs) caused simultaneous disinhibition of TRPV4 channels and suppression of Kir2.1 channels. These findings collectively support the concept that G$_q$PCR activation functions as a molecular switch to favor capillary TRPV4 activity over Kir2.1 signaling, an observation with potentially profound significance for the control of cerebral blood flow.

DOI: https://doi.org/10.7554/eLife.38689.001

*For correspondence:
Mark.Nelson@uvm.edu

Introduction

Endothelial cells (ECs) line the lumen of all blood vessels and are important regulators of artery and arteriole smooth muscle contractility. In capillaries, which lack an overlying smooth muscle cell layer, this regulatory function is absent. In these smallest of all blood vessels, ECs instead support the nutrient- and gas-exchange function characteristic of capillary beds generally. In the brain, capillary ECs (cECs) also constitute the blood-brain barrier, reflecting the presence of tight junctions between adjacent cECs. Not surprisingly given these differing cellular missions, the molecular repertoire of brain cECs and arterial/arteriolar ECs exhibit some marked differences. Notably, intermediate and small-conductance Ca^{2+}-activated K$^+$ channels (IK and SK, respectively), which are important in transducing elevations in intracellular Ca^{2+} concentration ([Ca^{2+}]$_i$) into membrane potential hyperpolarization in artery/arteriolar ECs to cause relaxation of electrically coupled smooth muscle cells (*Ledoux et al., 2008*; *Sonkusare et al., 2012*; *Taylor et al., 2003*), are absent in brain cECs (*Longden et al., 2017*). However, signaling through G protein–coupled receptors of the Gα$_{q/11}$-subtype (G$_q$PCRs)—an important component of this smooth muscle regulatory axis—is robust in brain cECs (*Harraz et al., 2018*). In the canonical pathway of G$_q$PCR signaling, Gα$_q$ released upon agonist binding activates phospholipase C (PLC), which hydrolyzes the minor inner leaflet phospholipid, phosphatidylinositol 4,5-bisphosphate (PIP$_2$). Breakdown of PIP$_2$ yields diacylglycerol (DAG) and inositol 1,4,5-trisphosphate (IP$_3$), the latter of which increases [Ca^{2+}]$_i$ by acting on its cognate receptor (IP$_3$R) on the endoplasmic reticulum (ER) to promote Ca^{2+} release from intracellular stores.

Blood delivery within the brain is mediated by an ever-narrowing vascular tree comprising surface arteries, penetrating (parenchymal) arterioles and a vast network of capillaries, which enormously

eLife digest Capillaries form branching networks that surround all cells of the body. They allow oxygen and nutrient exchange between blood and tissue, but this is not their only role. Capillaries in the brain form a tight barrier that prevents components carried in the blood from easily reaching the brain compartment. They also detect the activity of neurons and trigger on-demand increases in blood flow to active regions of the brain. This role, revealed only recently, depends upon ion channels on the surface of the capillary cells. Active neurons release potassium ions, which open a type of ion channel called Kir2.1 that allows potassium inside the cell to flow out. This process is repeated in neighboring capillary cells until it reaches an upstream vessel, where it causes the vessel to relax and increase the blood flow.

Kir2.1 channels sit astride the membranes of capillary cells, where they can interact with other membrane molecules. One such molecule, called PIP_2, plays several roles in relaying signals from the outside to the inside of cells. It also physically interacts with channels in the membrane, including Kir2.1 channels. If PIP_2 levels are low, Kir2.1 channel activity decreases.

Here, Harraz et al. discovered that capillary cells contain another type of ion channel, called TRPV4, which is also regulated by PIP_2. But unlike Kir2.1, its activity increases when PIP_2 levels drop. Moreover, TRPV4 channels allow sodium and calcium ions to flow into the cell, which has an effect opposite to that of potassium flowing out of the cell.

Capillary cells also have receptor proteins called G_qPCRs that are activated by chemical signals released by active neurons in the brain. G_qPCRs break down PIP_2, so their activity turns Kir2.1 channels off and TRPV4 channels on. This resets the system so that it is ready to respond to new signals from active neurons. G_qPCRs work as molecular switches to control the balance between Kir2.1 and TRPV4 channels and turn brain blood flow up and down.

G_qPCRs and ion channels that depend on PIP_2 can also be found in other types of cells. These findings could reveal clues about how signals are switched on and off in different cells. Understanding the role of PIP_2 in signaling could also unveil what happens when signaling go wrong.

extend the territory of perfusion (*Blinder et al., 2013*). Because the brain lacks substantial energy reserves, it relies on an on-demand mechanism for redistributing oxygen and nutrients to regions of higher neuronal activity, a process in which products released by active neurons trigger a local increase in blood flow. This use-dependent increase in local blood flow (functional hyperemia), mediated by a process termed neurovascular coupling (NVC), is essential for normal brain function (*Iadecola and Nedergaard, 2007*) and represents the physiological basis for functional magnetic resonance imaging (*Raichle and Mintun, 2006*).

We recently reported that brain capillaries act as a neuronal activity-sensing network, demonstrating that brain cECs are capable of initiating an electrical (hyperpolarizing) signal in response to neuronal activity that rapidly propagates upstream to dilate feeding parenchymal arterioles and increase blood flow locally at the site of signal initiation (*Longden et al., 2017*). We also established the molecular mechanism underlying this process, showing that extracellular K^+—a byproduct of every neuronal action potential—is the critical mediator and identifying the Kir2.1 channel as the key molecular player (*Longden et al., 2017*). Kir2.1 channels are activated by external K^+ and exhibit steep activation by hyperpolarization (*Hibino et al., 2010*; *Longden and Nelson, 2015*), characteristics that facilitate regenerative K^+ conductance in neighboring cECs and enable long-range propagation of the hyperpolarizing signal (*Longden et al., 2017*). Intriguingly, we have since discovered that decreases in capillary endothelial PIP_2 levels induced by G_qPCRs agonists suppress Kir2.1 channel currents, reflecting the fact that PIP_2 is required for Kir2.1 channel activity (*Harraz et al., 2018*). Importantly, this suppressive effect of PIP_2 depletion exerts a major modulatory influence on K^+-evoked hyperemic responses in vivo. In addition to regulating Kir2 family members, PIP_2 has been shown to bind to and regulate a diverse array of ion channels (*Hille et al., 2015*). Notable in this context, PIP_2 binding has been shown to inhibit several members of the transient receptor potential (TRP) family of non-selective cation channels, including the vanilloid subtype TRPV4 (*Nilius et al.,*

2008; *Rohacs, 2009*; *Takahashi et al., 2014*), which we and others have shown is an important Ca^{2+} influx pathway in arterial and arteriolar ECs (*Earley and Brayden, 2015*; *Sonkusare et al., 2014*; *Sonkusare et al., 2012*; *White et al., 2016*).

The Kir2.1 channel appears to be the major K^+ channel type in brain cECs (*Longden et al., 2017*). However, the identity of depolarizing (Na^+/Ca^{2+}-permeable) channels in cECs is not known. Here, we show that TRPV4 channels are present in cECs and exhibit an exceedingly low open probability under basal conditions due to tonic inhibition by PIP_2. We have further found that this inhibition is relieved through PIP_2 depletion, independent of the action of the PIP_2 hydrolysis products, DAG and IP_3. These findings provide a counterpoint to our recent demonstration that Kir2.1 channel activity is sustained by basal levels of PIP_2 and suppressed by G_qPCR-mediated PIP_2 depletion (*Harraz et al., 2018*). Collectively, our findings indicate that PIP_2 exerts opposite effects on TRPV4 and Kir2.1 channels in brain cECs, demonstrating that a single regulatory pathway governs the balance between two divergent signaling modalities—one depolarizing and the other hyperpolarizing—in the capillary endothelium.

Results

TRPV4 channels in brain cECs are inhibited by intracellular ATP

We previously reported that the selective TRPV4 agonist GSK1016790A (hereafter GSK101) is a potent activator of TRPV4 currents in mesenteric artery ECs that induces maximal arterial dilation at concentrations in the low nanomolar range (*Sonkusare et al., 2014*; *Sonkusare et al., 2012*). To assess TRPV4 channel expression and function in brain cECs, we first performed patch-clamp electrophysiology experiments on freshly isolated cECs from C57BL/6J mouse brain slices, prepared as described in Materials and methods. Specifically, we recorded outward K^+ currents mediated by TRPV4 channels in the cytoplasm-intact, perforated whole-cell configuration using a 300 ms ramp protocol (−100 to +100 mV, from a holding potential of −50 mV). Recordings were made in the presence of the voltage-dependent pore blocker ruthenium red (RuR; 1 µM), an approach we have previously used to assess TRPV4 currents in mesenteric artery ECs (*Sonkusare et al., 2012*). Under these conditions, depolarizing ramps rapidly displace RuR, allowing unimpeded outward K^+ currents to be detected while preventing Na^+/Ca^{2+} influx and associated Ca^{2+} overload and cell death (*Sonkusare et al., 2012*). Unexpectedly, we found that GSK101 was unable to evoke a detectable whole-cell TRPV4 current in cECs at concentrations that maximally activate TRPV4 channels in mesenteric artery ECs; in fact, even GSK101 concentrations as high as 100 nM failed to stimulate a detectable TRPV4 current in isolated cECs (*Figure 1A*). However, we serendipitously found that breaking through the cell membrane from a perforated patch in the presence of an otherwise ineffective GSK101 concentration (100 nM) resulted in the gradual (~5 min) development of a robust TRPV4 current, suggesting that a factor that suppresses TRPV4 channels had been washed out of the cell.

In the conventional whole-cell configuration with physiological levels of Mg-ATP (1 mM) included in the patch pipette, application of 100 nM GSK101 also failed to evoke an outward current. In striking contrast, this same concentration of GSK101 caused the gradual (~4–5 min) development of a robust outward current in the conventional whole-cell configuration when Mg-ATP was omitted from the pipette solution (*Figure 1A*). Collectively, these observations suggest that ATP is the suppressive factor in question. Consistent with this interpretation, intracellular Mg-ATP (1 mM) caused a dramatic shift in the sensitivity of cEC TRPV4 channels to GSK101: at a potential of 100 mV, the EC_{50} of GSK101 for TRPV4 channels in the presence of Mg-ATP was 415 nM. However, in the absence of Mg-ATP, the EC_{50} was reduced ~23 fold to 18 nM (*Figure 1C*; *Figure 1—figure supplement 1A,B*), a value comparable to that observed in mesenteric artery ECs (*Sonkusare et al., 2014*). The suppressive effect of ATP was specific for adenosine nucleotides, as inclusion of 1 mM GTP in the patch pipette did not alter currents (*Figure 1—figure supplement 1C*). GSK101-induced currents were completely abolished by the selective TRPV4 channel antagonist HC-067047 (1 µM) and were absent in cECs from TRPV4-knockout (TRPV4$^{-/-}$) mice (*Figure 1B*; *Figure 1—source data 1*), confirming that these currents are attributable to TRPV4 channels. The inhibitory effect of intracellular Mg-ATP (1 mM) was not limited to GSK101-activated TRPV4 currents. As shown (*Figure 1—figure supplement*
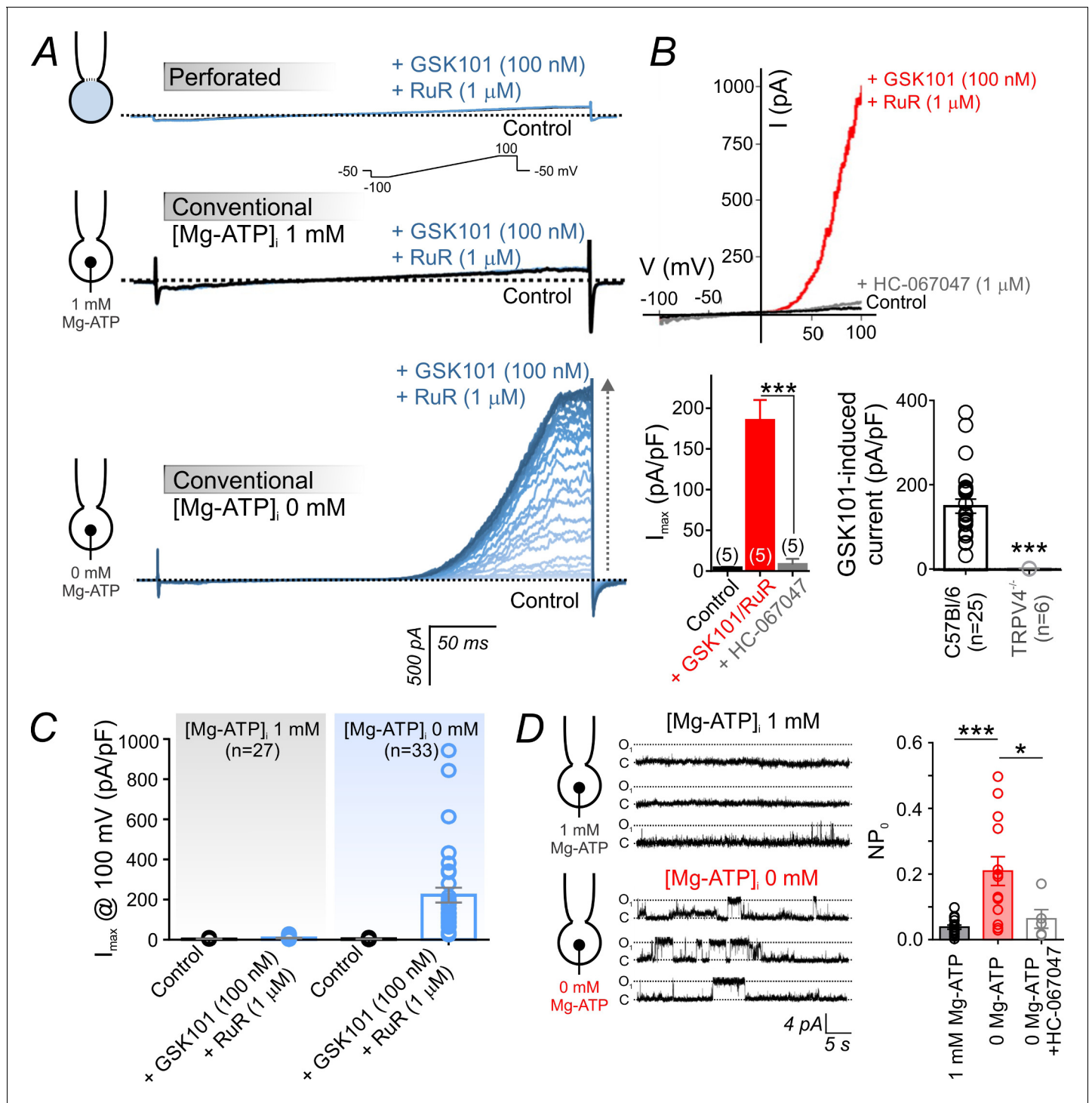
Figure 1. Intracellular ATP suppresses TRPV4 currents in cECs. (**A**) Representative traces of TRPV4 currents recorded from freshly isolated cECs using voltage ramps (−100 to 100 mV, from a holding potential −50 mV; inset) and different patch-clamp configurations before (black) and after (blue) the application of 100 nM GSK101 and 1 μM RuR. *Top*: Currents recorded in the perforated whole-cell configuration. *Middle*: Currents recorded in the conventional whole-cell configuration (dialyzed cytoplasm, 1 mM Mg-ATP in the pipette solution). *Bottom*: Currents recorded in the conventional whole-cell configuration (0 mM Mg-ATP in the pipette solution) developed gradually over ~4 min. (**B**) Current-voltage relationship (*top*) and summary data (*bottom left*) of currents recorded before (control) and after the cumulative application of GSK101 (100 nM)+RuR (1 μM) followed by HC-067047 (1 μM) (means ± SEM, ***p<0.001, unpaired Student's t-test; n = 5 each). *Bottom right*: Individual-value plot of peak outward GSK101 (100 nM)-induced currents in cECs isolated from brains of C57Bl/6 (n = 25) or TRPV4$^{-/-}$ (n = 6) mice. A minimum duration of ~5 min after the application of GSK101 was allowed for outward TRPV4 current to develop in each cEC. Data are presented as means ± SEM (***p<0.001, unpaired Student's t-test). (**C**) Individual-

Figure 1 continued on next page

2), it also suppressed both inward and outward currents in cECs activated by the TRPV4 agonist 4α-phorbol 12,13-didecanoate (4α-PDD; 5 μM, in the absence of RuR).

There was no detectable whole-cell TRPV4 current in the absence of a TRPV4 activator (*Figure 1A*), suggesting that these channels have a very low basal open probability. To further investigate this, we monitored single TRPV4 channel openings using dialyzed cECs in the conventional whole-cell configuration, an approach that should allow detection of openings of all channels throughout the cEC plasma membrane while controlling intracellular composition. First, we measured TRPV4 unitary currents in dialyzed cECs (0 mM Mg-ATP) held at +50 mV before and after the application of 100 nM GSK101. The unitary current amplitude in the presence of GSK101, estimated from amplitude histograms, was 4.6 ± 0.3 pA (n = 3) (*Figure 1—figure supplement 3A*). This value corresponds to a single-channel conductance of 92 ± 6 pS, in line with values reported in an earlier investigation of TRPV4 channels in native arterial ECs (*Watanabe et al., 2002*) and heterologous expression systems (*Loukin et al., 2010*). Extending these results, we next performed a series of single-channel recordings in the absence of GSK101. cECs held at +50 mV and dialyzed with Mg-ATP (1 mM) displayed infrequent openings (NP_O = 0.038 ± 0.006), but removing ATP increased single-channel opening by ~6 fold (NP_O = 0.209 ± 0.044) (*Figure 1D*; *Figure 1—source data 3*). Single-channel openings in the absence of agonist exhibited a unitary current of 4.5 ± 0.3 pA at +50 mV (*Figure 1D*, *Figure 1—figure supplement 3B*), similar to that evoked using a specific TRPV4 agonist (4.6 pA) (*Figure 1—figure supplement 3A*) and corresponding to a conductance of 90 ± 6 pS. Single-channel currents recorded in the absence of GSK101 were inhibited by the TRPV4 blocker HC-067047 (NP_O = 0.063 ± 0.028) (*Figure 1D*; *Figure 1—source data 3*), confirming their identity as TRPV4 channel-mediated currents. Based on our estimate of ~225 functional TRPV4 channels per cEC (see Materials and methods), we calculate that capillary TRPV4 channels have a basal open probability (P_O) of ~0.0002. These observations collectively indicate that capillary TRPV4 channels exhibit a low open probability under basal conditions, and that both constitutive and agonist-induced TRPV4 activities are suppressed by intracellular ATP and recover following ATP washout/dialysis.

TRPV4 channel suppression is dependent on ATP hydrolysis, but independent of protein kinase A, G or C

The Mg^{2+} salt of ATP is readily hydrolyzable and can be utilized by kinases (*O'Rourke, 1993*). To test whether TRPV4 suppression requires ATP hydrolysis, we replaced ATP in the patch pipette with

the poorly hydrolyzable analog, ATP-γ-S (1 mM). Under these conditions, GSK101 (100 nM) increased TRPV4 currents to same extent as observed in cells dialyzed with 0 mM Mg-ATP, indicating that ATP hydrolysis is required for channel inhibition (*Figure 2A,B*; *Figure 2—source data 1*). This implies an energy-consuming process, and suggests the involvement of an enzyme, possibly a
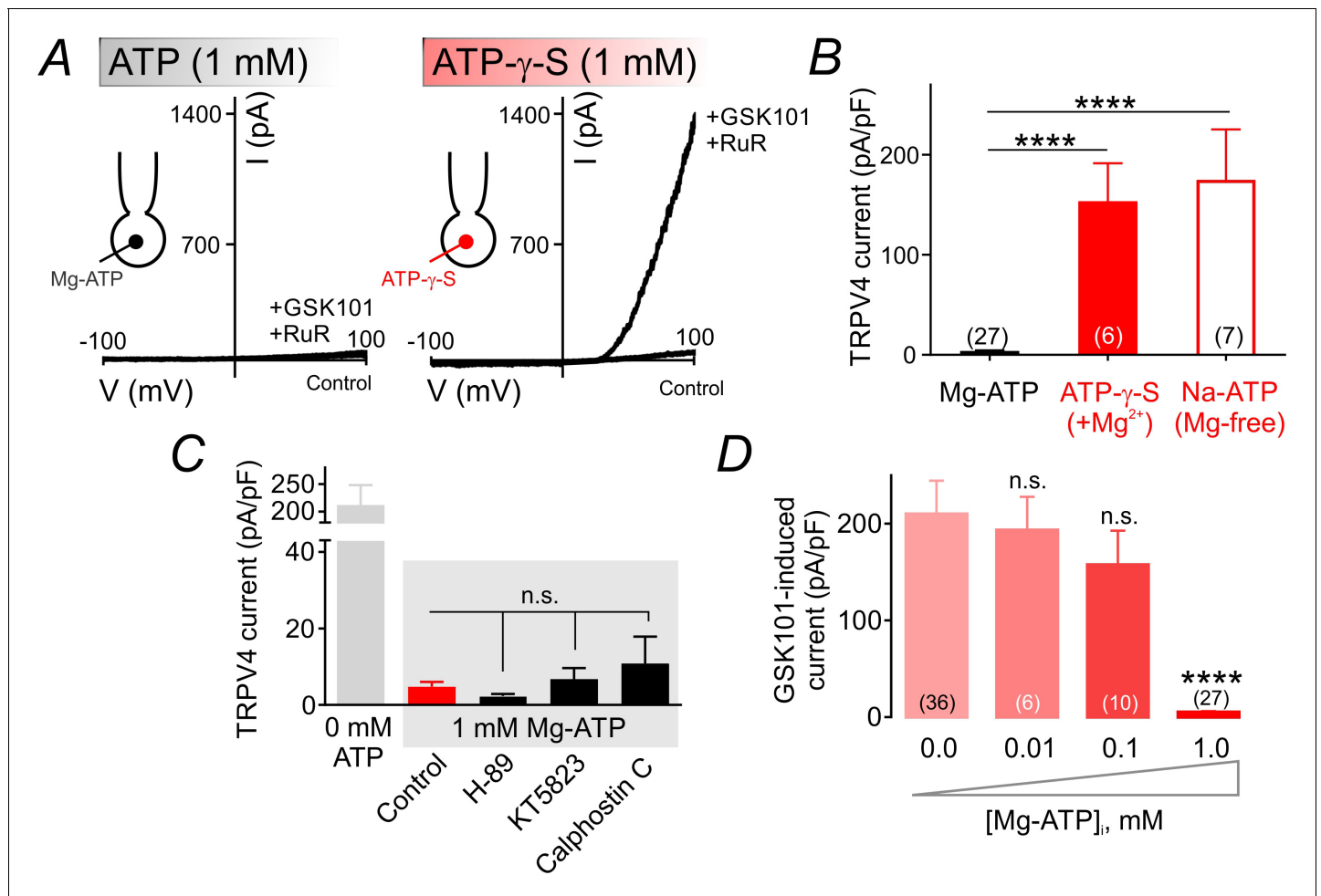

Figure 2. ATP hydrolysis is required for ATP-mediated suppression of TRPV4 channel activity. (A) Representative traces of current-voltage relationships in cECs recorded using voltage ramps (−100 to 100 mV) before and after the application of 100 nM GSK101 and 1 μM RuR. cECs were dialyzed with 1 mM Mg-ATP (*left*) or 1 mM Mg-ATP-γ-S (*right*). (B) Summary data showing GSK101 (100 nM)-induced outward currents at 100 mV in cECs dialyzed with Mg-ATP (1 mM), Mg-ATP-γ-S (1 mM) or Na-ATP (1 mM, in Mg^{2+} free solution). A minimum duration of 5 min after the application of GSK101 was allowed for outward TRPV4 current to develop in each cEC. Data are presented as means ± SEM (****$p<0.0001$ vs. Mg-ATP, one-way ANOVA followed by Dunnett's multiple comparisons test). (C) TRPV4 outward currents induced by 100 nM GSK101 at 100 mV, recorded from dialyzed cECs (0 and 1 mM Mg-ATP). Mg-ATP–dialyzed cECs (gray shadow) were pre-treated with inhibitors of PKA (H-89, 1 μM), PKG (KT5823, 1 μM) or PKC (calphostin C, 0.5 μM) for ~10–15 min prior to GSK101 application, or left untreated (control). Data are presented as means ± SEM (n.s. denotes not significant vs. control Mg-ATP, one-way ANOVA, Dunnett's multiple comparisons test, n = 6–24). (D) Summary data showing the effect of raising intracellular Mg-ATP concentration on GSK101-induced TRPV4 currents. Data are means ± SEM (****$p<0.0001$, one-way ANOVA followed by Dunnett's multiple comparisons test).

kinase. Coordination of Mg^{2+} is critical for kinase-mediated phosphoryl transfer reactions (*O'Rourke, 1993*; *Ryves and Harwood, 2001*; *Zakharian et al., 2011*). Thus, the prediction is that ATP would be unable to inhibit TPRV4 currents in the absence of the cofactor Mg^{2+} if a kinase underlies Mg-ATP–mediated TRPV4 inhibition. Consistent with this prediction, replacing Mg-ATP in the patch pipette with the Na^+ salt of ATP (Na-ATP, 1 mM) while eliminating Mg^{2+} from the pipette solution abolished the suppressive effect of ATP (*Figure 2B*; *Figure 2—source data 1*), suggesting the contribution of a kinase to this process.

On the basis of these observations, we next tested the involvement of protein kinases by bath-applying the protein kinase A (PKA) inhibitor H-89 (1 µM), protein kinase G (PKG) inhibitor KT5823 (1 µM), or protein kinase C (PKC) inhibitor calphostin C (0.5 µM). We then monitored outward TRPV4-mediated currents as described above. None of these inhibitors affected currents in cells dialyzed with Mg-ATP (*Figure 2C*; *Figure 2—source data 2*), ruling out a role for these protein kinases in TRPV4 inhibition. Further support for this conclusion is provided by the observation that lower concentrations of Mg-ATP (10 and 100 µM)—which activate the majority of protein kinases (*Knight and Shokat, 2005*)—failed to effectively inhibit TRPV4 currents in cECs (*Figure 2D*; *Figure 2—source data 3*).

ATP-dependent suppression of TRPV4 channels is mediated by PIP_2

Lipid kinases, like protein kinases, also hydrolyze ATP, but typically require higher ATP concentrations (*Hilgemann, 1997*; *Knight and Shokat, 2005*; *Xie et al., 1999*). The requirement for millimolar Mg-ATP concentrations to effectively inhibit TRPV4 currents (*Figure 1C*, *Figure 2D*) is thus more consistent with lower ATP-affinity lipid kinases like those involved in phosphoinositide synthesis (*Balla and Balla, 2006*). In this cascade (*Figure 3A*), phosphatidylinositol 4-kinase (PI4K) utilizes ATP to phosphorylate phosphatidylinositol (PI), converting it to phosphatidylinositol 4-phosphate (PIP), which in turn is phosphorylated to PIP_2 by phosphatidylinositol 4-phosphate 5-kinase (PIP5K), a step that also requires ATP. Thus, the cellular levels of PIP_2 are maintained through an ATP-hydrolysis–dependent process (*Baukrowitz et al., 1998*; *Hilgemann, 1997*; *Suh and Hille, 2002*). To assess the possible involvement of this pathway in capillary TRPV4 suppression, we tested the effects of four structurally unrelated pharmacological inhibitors of PI4K: wortmannin (50 µM), PIK93 (300 nM), phenylarsine oxide (PAO; 30 µM), and LY294002 (300 µM). In each case, inhibitors of PIP_2 synthesis significantly reversed TRPV4 channel inhibition by ATP (*Figure 3B*; *Figure 3—source data 1*), despite the high intracellular Mg-ATP concentration (1 mM). Notably, at concentrations below those necessary to inhibit PI4K (but sufficient to suppress phosphoinositide 3-kinases), the inhibitors wortmannin (0.1 µM) and LY294002 (10 µM) failed to increase TRPV4 current in cECs (*Figure 3B*; *Figure 3—source data 1*). Collectively, these observations indicate the involvement of the ATP/PI4K regulatory axis, and presumably PIP_2, in suppressing TRPV4 channels in cECs.

PIP_2 is a well-established regulator of membrane proteins, including ion channels (*Hille et al., 2015*; *Huang et al., 1998*; *Nilius et al., 2008*). To directly test whether PIP_2 inhibits TRPV4 channels in cECs, we introduced the water-soluble, short acyl chain dioctanoyl PIP_2 (diC8-PIP_2) via the patch pipette. In the absence of Mg-ATP, diC8-PIP_2 inhibited GSK101-induced TRPV4 currents, reducing them by 70–80% at concentrations of 10 to 50 µM (*Figure 3C,D*; *Figure 3—source data 2*). Similar inhibition was observed with the longer-chain PIP_2 analog, diC16-PIP_2 (10 µM) (*Figure 3—figure supplement 1*). Moreover, scavenging endogenous, negatively charged PIP_2 with intracellular poly-L-lysine (3 µg/ml, molecular weight 15,000–30,000), included in the patch pipette, attenuated Mg-ATP effects on GSK101-induced TRPV4 currents (*Figure 3E,F*; *Figure 3—source data 3*). Taken together, these data show that PIP_2 inhibits both GSK101-induced and constitutive TRPV4 channel activity in cECs.

G_qPCR activation relieves TRPV4 suppression in cECs by promoting PIP_2 hydrolysis

The primary mechanism responsible for reducing PIP_2 levels is activation of G_qPCRs and subsequent PLC-mediated PIP_2 hydrolysis. To determine whether endothelial G_qPCR-activation–mediated PIP_2 depletion relieves the inhibition of TRPV4 channels, we examined the effects of G_qPCR agonists on constitutive single-channel TRPV4 currents in cECs under simulated physiological conditions (i. e. dialyzed with Mg-ATP) (*Figure 1D*). We first tested the effects of prostaglandin E2 (PGE_2), a
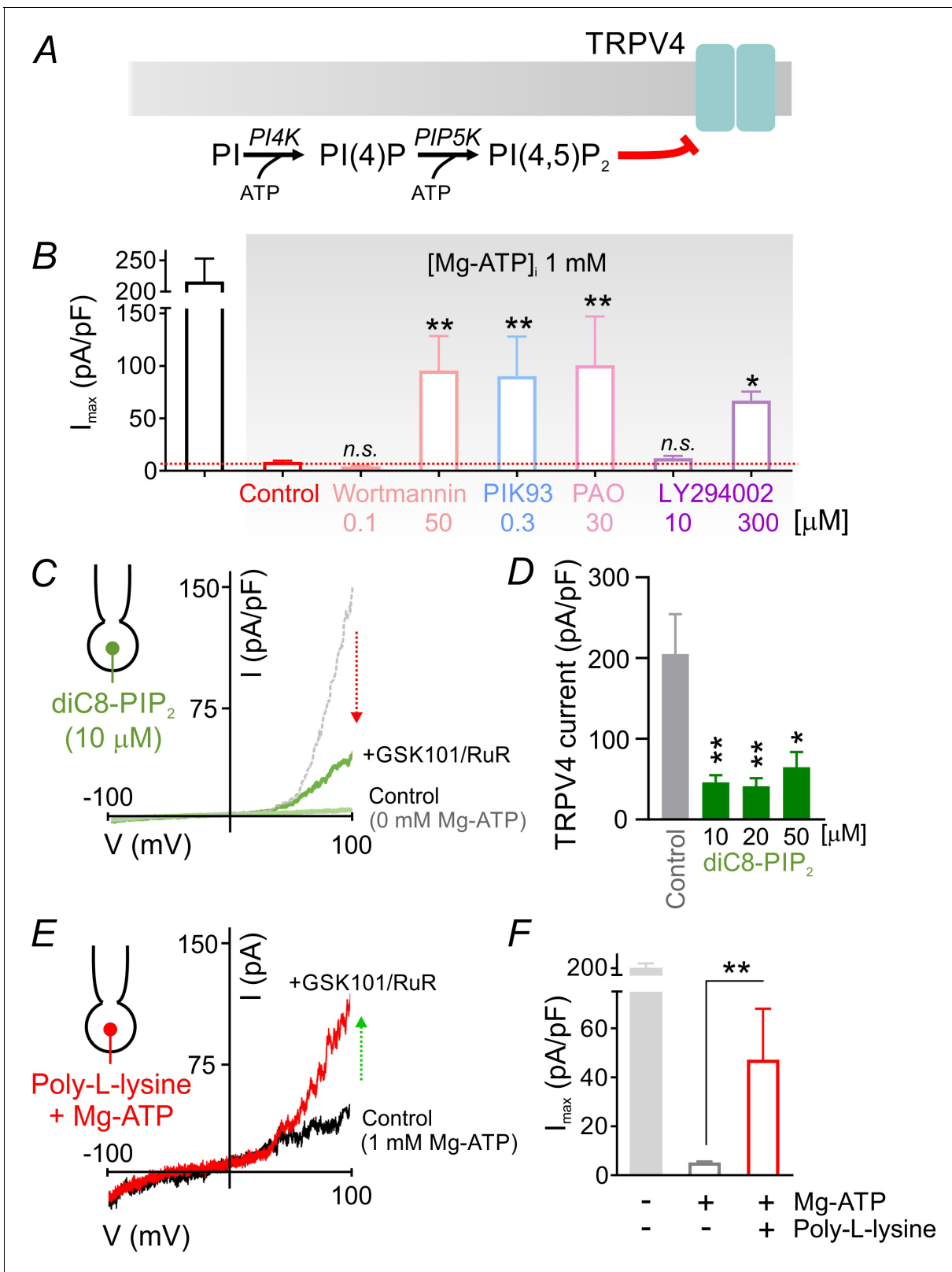
Figure 3. PIP$_2$ mediates tonic inhibition of capillary TRPV4 channels. (**A**) Schematic diagram showing the ATP-dependent synthesis steps leading to the production of PIP$_2$. (**B**) Average maximum outward TRPV4 current induced by 100 nM GSK101, recorded in cECs at 100 mV using the conventional whole-cell configuration. cECs dialyzed with 1 mM Mg-ATP were treated for ~10 min with wortmannin (0.1, 50 µM), PIK93 (0.3 µM), PAO (30 µM) or LY294002 (10, 300 µM), or were left untreated (control). A minimum duration of 10–15 min after the application of GSK101 was allowed for outward

Figure 3 continued on next page

Figure 3 continued

TRPV4 current to develop in each cEC. Data are means ± SEM (**p<0.01, *p<0.05 vs. control Mg-ATP, one-way ANOVA followed by Dunnett's multiple comparisons test; n = 6–27). (C) Traces of current-voltage relationship obtained from a cEC dialyzed with 10 μM diC8-PIP$_2$ and 0 mM Mg-ATP using a voltage ramp (−100 to 100 mV) before and after (green) the application of GSK101 (100 nM) and RuR (1 μM). The dotted gray trace is a representative GSK101-induced current recorded from a control cEC dialyzed with 0 μM diC8-PIP$_2$ and 0 mM Mg-ATP. (D) Summary data showing GSK101 (100 nM)-induced currents at 100 mV in cECs dialyzed with different concentrations of diC8-PIP$_2$ (10, 20, 50 μM) or 0 μM phosphoinositide (control). The pipette solution lacked Mg-ATP in all groups. GSK101-evoked outward currents developed over ~5 min. Data are presented as means ± SEM (*p<0.05, **P<0.01, one-way ANOVA followed by Dunnett's multiple comparisons test; n = 10–18). (E, F) Representative trace (E) and summary data showing GSK101-induced currents in cECs dialyzed with 1 mM Mg-ATP and poly-L-lysine (3 μg/ml). A duration of 10 min was allowed after the application of GSK101 for outward TRPV4 current to develop in each cEC. Data in F are presented as means ± SEM (**p<0.01, unpaired Student's t-test; n = 8–18).
DOI: https://doi.org/10.7554/eLife.38689.014

The following source data and figure supplements are available for figure 3:

Source data 1. Numerical data that were used to generate the chart in *Figure 3B*.
DOI: https://doi.org/10.7554/eLife.38689.017
Source data 2. Numerical data that were used to generate the chart in *Figure 3D*.
DOI: https://doi.org/10.7554/eLife.38689.018
Source data 3. Numerical data that were used to generate the chart in *Figure 3F*.
DOI: https://doi.org/10.7554/eLife.38689.019
Figure supplement 1. The long-acyl chain PIP$_2$, diC16-PIP$_2$, suppresses TRPV4 currents.
DOI: https://doi.org/10.7554/eLife.38689.015
Figure supplement 2. 11,12-EET-induced currents in cECs.
DOI: https://doi.org/10.7554/eLife.38689.016

postulated NVC agent that acts on G$_q$-coupled EP$_1$ receptors in cECs to deplete PIP$_2$ (*Harraz et al., 2018*) and has previously been proposed to act through G$_s$-protein-coupled EP$_2$ and EP$_4$ receptors to cause vasodilation (*Lacroix et al., 2015*; *Zonta et al., 2003*). PGE$_2$ significantly increased TRPV4 single-channel open probability in the absence of GSK101 (*Figure 4A,B*), increasing NP$_O$ ~6 fold (*Figure 4C*; *Figure 4—source data 1*). This enhancement was similar to that observed under conditions in which intracellular Mg-ATP was excluded from the pipette solution (in the absence of either a receptor agonist or GSK101; *Figure 1D*), suggesting that PGE$_2$ acts through PIP$_2$ depletion to relieve PIP$_2$-mediated inhibition and restore TRPV4 channel activity.

To confirm that PIP$_2$ depletion underlies PGE$_2$-induced activation of TRPV4 channels, we next employed a series of conventional whole-cell recordings and pharmacological interventions to test the different components in the proposed pathway. In these experiments, cECs were dialyzed with 1 mM Mg-ATP—a maneuver sufficient to significantly suppress TRPV4 channels even in the presence of 100 nM GSK101 (*Figure 1A,C*). As predicted, application of PGE$_2$ (2 μM) in the presence of GSK101 greatly increased TRPV4 currents in cECs dialyzed with Mg-ATP (*Figure 5A,B*; *Figure 5—source data 1*). Currents evoked by PGE$_2$ application were inhibited by the TRPV4 antagonist HC-067047 (1 μM) and were absent in cECs from TRPV4$^{-/-}$ animals, confirming that they are mediated by TRPV4 channels (*Figure 5C*; *Figure 5—figure supplement 1*). Introduction of the PIP$_2$ analog diC8-PIP$_2$ (10 μM) in the pipette solution or inhibition of PLC using U73122 (10 μM)—pharmacological interventions that serve to compensate for or prevent PLC-dependent PIP$_2$ degradation, respectively—prevented the increase in TRPV4 currents by PGE$_2$ (*Figure 5C*; *Figure 5—figure supplement 1*; *Figure 5—source data 2*). The non-selective prostanoid receptor (EP$_1$/EP$_2$/EP$_3$) antagonist AH6809 (10 μM) also prevented this effect of PGE$_2$, as did the selective EP$_1$ antagonist SC51322 (1 μM), suggesting that PGE$_2$ acts through the EP$_1$ receptor. U73343, the inactive analog of the PLC inhibitor U73122, did not alter PGE$_2$ effects (*Figure 5C*; *Figure 5—source data 2*). Collectively, these observations suggest that PGE$_2$ signals through the EP$_1$-PLC pathway to deplete PIP$_2$ and thereby relieve PIP$_2$-mediated TRPV4 inhibition.

The PIP$_2$ breakdown products, DAG and IP$_3$, stimulate PKC activity and promote Ca^{2+} release from the endoplasmic reticulum, respectively. To rule out the involvement of these pathways in the PGE$_2$-induced increase in TRPV4 currents, we first tested the effects of the PKC inhibitors, Gö6976 (1 μM) and calphostin C (0.5 μM), and found that neither altered PGE$_2$-induced activation of TRPV4 channels (*Figure 5C*; *Figure 5—source data 2*). To determine whether intracellular Ca^{2+} signals downstream of EP$_1$-PLC activation by PGE$_2$ are involved in TRPV4 disinhibition, we blocked Ca^{2+}

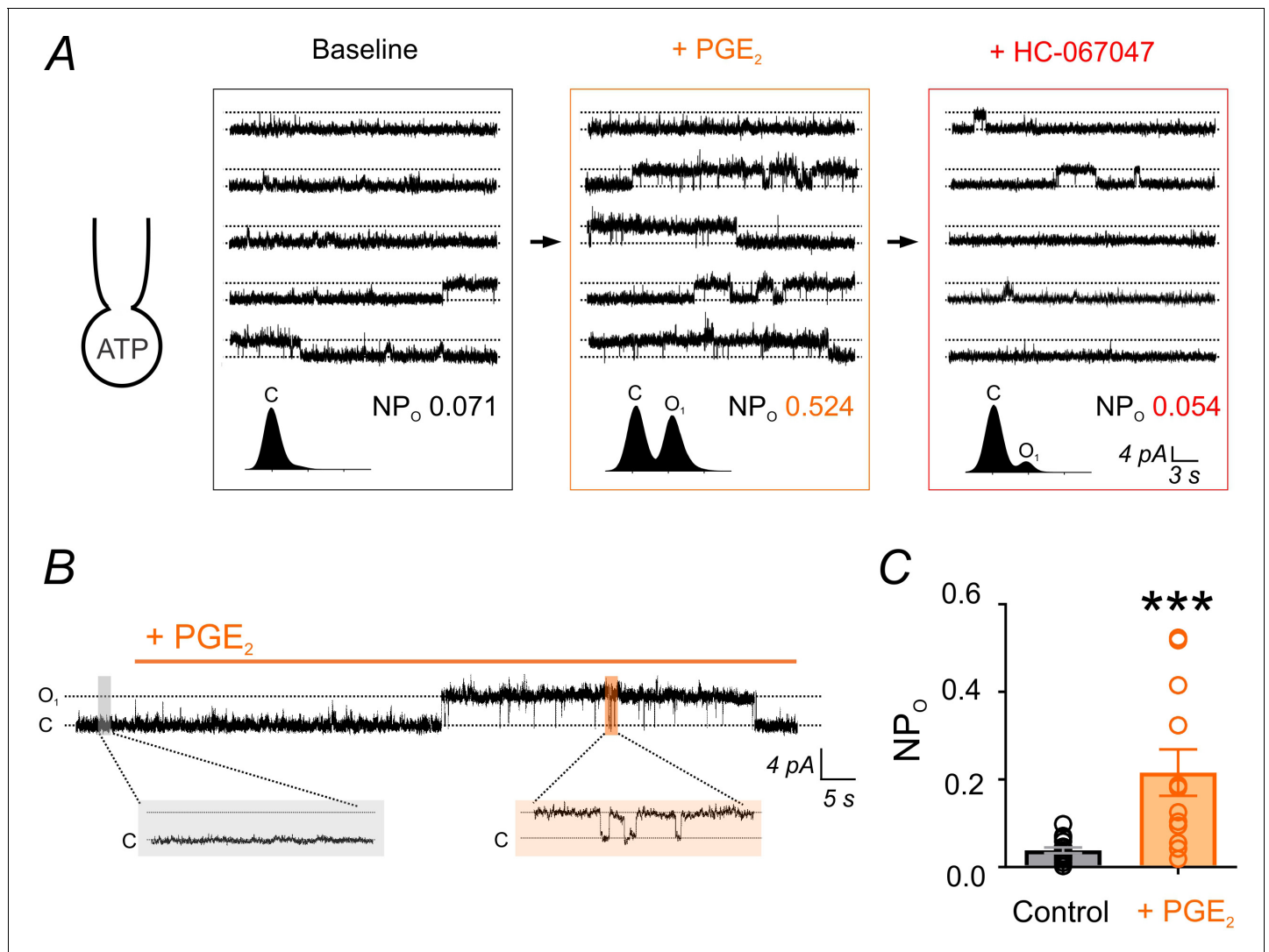**Figure 4.** PGE$_2$ enhances TRPV4 channel activity. (**A**) *Top:* Representative conventional whole-cell recordings from a cEC dialyzed with 1 mM Mg-ATP in the absence of GSK101 and held at a membrane potential of +50 mV. Quantal outward K$^+$ currents (unitary current, 4.6 pA; sampling rate, 20 kHz; lowpass filter frequency, 1 kHz), reflecting single-channel openings, were recorded before (baseline) and after the consecutive application of PGE$_2$ (2 μM) and HC-067047 (1 μM). *Bottom:* Corresponding amplitude histograms and open probability (NP$_O$) values. (**B, C**) Representative trace (**B**) and individual-value plot (**C**) of TRPV4 NP$_O$ in cECs (dialyzed with 1 mM Mg-ATP, held at +50 mV) in the absence (control; n = 16) and presence (n = 12) of 2 μM PGE$_2$. Data in *C* are means (column bars) ± SEM (error bars, ***p<0.001, unpaired Student's t-test). Each data point represents a recording from a cEC; the average duration of each recording was 5 min.

The following source data is available for figure 4:

reuptake into intracellular stores by inhibiting the sarcoplasmic/endoplasmic reticulum Ca^{2+} ATPase (SERCA) pump with cyclopiazonic acid (CPA; 30 μM) or by rapidly chelating cytoplasmic Ca^{2+} with BAPTA (5.4 mM). Neither maneuver attenuated PGE$_2$-induced disinhibition of TRPV4 channel activity (*Figure 5C*; *Figure 5—source data 2*), arguing against a major contribution of DAG-PKC or IP$_3$-Ca^{2+} signaling to this effect. Taken together, our data show that PGE$_2$ activates EP$_1$ receptors and downstream PLC to deplete PIP$_2$ and thereby relieve TRPV4 channel inhibition, independently of PIP$_2$ metabolites.
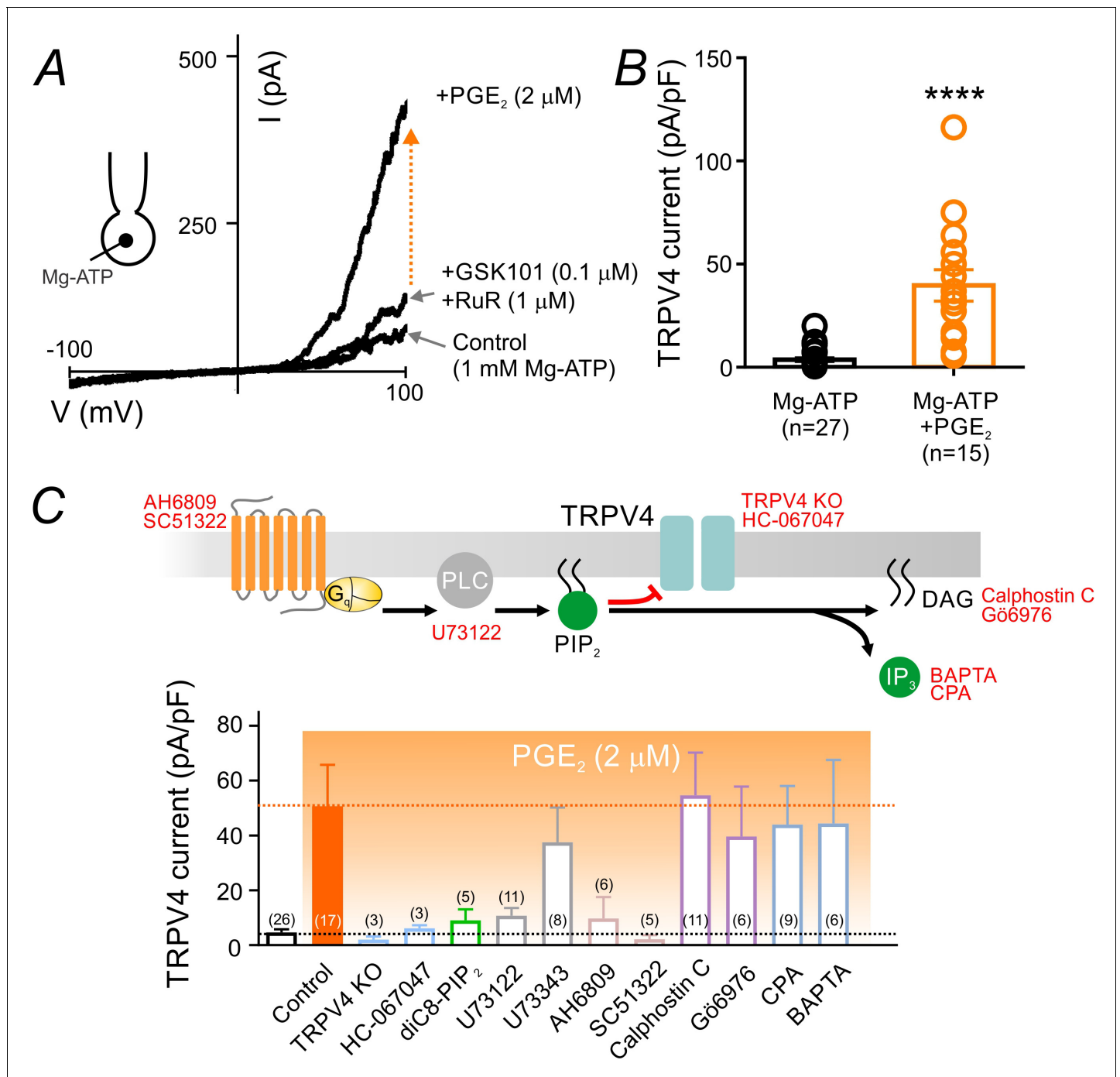
Figure 5. PGE$_2$ relieves PIP$_2$-mediated TRPV4 channel suppression. (**A**) Representative current-voltage plots obtained from a cEC dialyzed with 1 mM Mg-ATP and treated consecutively with GSK101 (100 nM) and RuR (1 μM) followed by 2 μM PGE$_2$. (**B**) Summary individual-value plot of GSK101-induced TRPV4 currents at 100 mV in cECs dialyzed with 1 mM Mg-ATP in the absence (black; n = 27) and presence (orange; n = 15) of 2 μM PGE$_2$. Incubation of cECs with PGE$_2$ lasted ~15 min. Data in *B* are means (column bars) ± SEM (error bars, ****p<0.0001, unpaired Student's t-test). (**C**) *Top:* Schematic diagram showing the G$_q$PCR-dependent hydrolysis of PIP$_2$ and the interventions used to test different components of the proposed pathway. *Bottom:* Summary data showing GSK101 (100 nM)-induced currents recorded at 100 mV in cECs dialyzed with 1 mM Mg-ATP. Currents were recorded in the absence and presence of 2 μM PGE$_2$ (orange shading), with or without (control) the indicated interventions. Concentrations (and application method): HC-067047, 1 μM (bath); diC8-PIP$_2$, 10 μM (pipette), U73122, 10 μM (bath); U73343, 10 μM (bath); AH6809, 10 μM (bath); SC51322, 1 μM (bath); calphostin C, 0.5 μM (bath); Gö6976, 1 μM (bath); CPA, 30 μM (bath); BAPTA, 5.4 mM (pipette). For bath application, pharmacological agents were added 10–15 min before PGE$_2$ application.

Figure 5 continued on next page

Carbachol (10 µM), which can signal through G$_q$-coupled muscarinic receptors, induced an increase in TRPV4 currents comparable to that produced by PGE$_2$ (*Figure 5—figure supplement 2*), indicating that G$_q$PCR-mediated TRPV4 activation is not restricted to prostanoid EP$_1$ receptors. However, neither the purinergic receptor agonist, ATP (50 µM), nor the protease-activated receptor-2 (PAR2)-activating peptide, SLIGRL-NH$_2$ (5 µM), affected TRPV4 channel activity (*Figure 5—figure supplement 2*). The reason for these apparent differential effects of various G$_q$PCRs is currently unclear, but could reflect differences in expression levels or cellular localization of the corresponding receptors, or receptor desensitization owing to ligand-dependent proteolysis (PAR2) or receptor internalization (e.g. P2Y subtypes)(*Cho et al., 2005a, 2005b*; *Dickson et al., 2013*; *Jung et al., 2016*; *Sromek and Harden, 1998*; *Vanlandewijck et al., 2018*).

G$_q$PCR signaling as a 'switch' that shifts the balance between TRPV4 and Kir2.1 signaling

PIP$_2$ levels are key to the maintenance and activation of inward rectifier K$^+$ channels, as reported recently by our group (*Harraz et al., 2018*) and others (*D'Avanzo et al., 2010*; *Hansen et al., 2011*; *Huang et al., 1998*). Our current (*Figure 5*) and previous (*Harraz et al., 2018*) findings indicate that G$_q$PCR-activation–induced depletion of PIP$_2$ exerts opposite effects on endothelial TRPV4 (*activation*) and Kir2.1 (*inhibition*) channels. In fact, G$_q$PCR activation in cECs deactivates Kir2.1 currents through PIP$_2$ hydrolysis and cripples capillary-to-arteriolar electrical signaling (*Harraz et al., 2018*). It is thus conceivable that G$_q$PCR-mediated signaling could shift the balance between TRPV4 and Kir2.1 signaling in brain capillaries through perturbation of endothelial PIP$_2$ levels. To test this, we designed an experiment that allowed simultaneous monitoring of TRPV4 and Kir2.1 currents in the context of G$_q$PCR-mediated changes in endothelial PIP$_2$ levels. Using the perforated-patch configuration to maintain physiological levels of ATP and PIP$_2$, and bathing cECs in a solution containing an extracellular K$^+$ concentration ([K$^+$]$_o$) of 60 mM to facilitate monitoring of Kir2.1 currents, we evoked TRPV4 currents with 2 µM GSK101, a concentration sufficient to sub-maximally activate an outward current in this configuration (in the presence of 1 µM RuR to block inward TRPV4 current). In this setting, application of PGE$_2$ (2 µM) enhanced TRPV4 currents and simultaneously inhibited Kir2.1 currents (*Figure 6A,B*; *Figure 6—source data 1*) compared with matching time controls, which showed no significant change in either current (*Figure 6—figure supplement 1*). The onset of changes in TRPV4 and Kir2.1 currents in response to PGE$_2$ was rapid (<60 s). A kinetic analysis revealed that TRPV4 activation and Kir2.1 suppression were kinetically comparable, with times for half-maximal change in activity ($t_{0.5}$) of 3.4 min for TRPV4 and 4.4 min for Kir2.1 channels, and corresponding time constants (τ) of 4.9 and 6.4 min, respectively (*Figure 6C*; *Figure 6—source data 2*). The muscarinic receptor agonist carbachol (10 µM) similarly facilitated TRPV4 currents and inhibited Kir2.1 currents (*Figure 6—figure supplement 2*). In contrast, purinergic receptor stimulation with ATP did not affect TRPV4 currents (*Figure 5—figure supplement 2*; *Figure 6—figure supplement 3*) despite inhibiting Kir2.1 currents (*Figure 6—figure supplement 3*), as we reported previously (*Harraz et al., 2018*). These findings collectively establish a potential mechanism by which PGE$_2$ or other suitable G$_q$PCR agonists, could alter the balance between electrical (hyperpolarizing) signaling mediated by Kir2.1 channels and TRPV4 channel signaling in capillaries through modulation of PIP$_2$ levels (*Figure 7*).
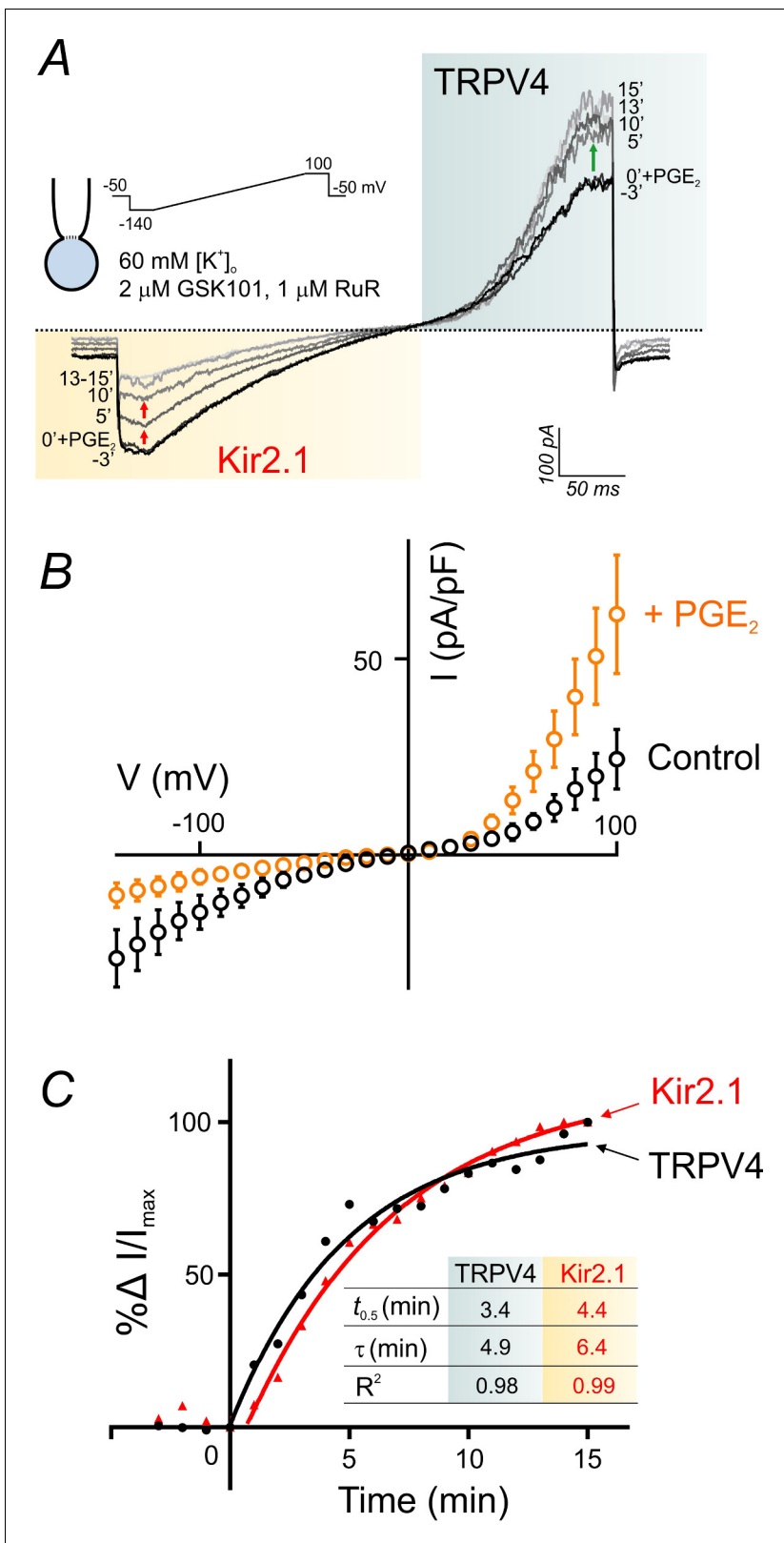
Figure 6. PGE$_2$ simultaneously and reciprocally regulates TRPV4 and Kir2.1 channel activities. (**A**) Representative traces illustrate simultaneous recordings of Kir2.1 (inward) and TRPV4 (outward) currents in a cEC obtained using the perforated whole-cell configuration. Voltage ramps (300 ms, −140 to 100 mV) were used and the cEC was bathed in a 60 mM [K$^+$]$_o$ solution supplemented with 2 μM GSK101 and 1 μM RuR. Traces represent currents before and for a duration of 15 min after the application of 2 μM PGE$_2$. (**B**) Averaged current-voltage relationship (n = 5 cECs) corresponding

Figure 6 continued on next page

Figure 6 continued

to the experiment in *A*, before (control) and after (maximum changes at 15 min) application of PGE_2. (**C**) Summary data showing the kinetics of TRPV4 current enhancement (black) and Kir2.1 current decline (red) following application of 2 μM PGE_2 onto cECs (as in *A*) at room temperature. Points are average percentage change in normalized currents before and over 15 min after PGE_2 application (n = 5). Curves are best fits of exponential change (rise: TRPV4; decay: Kir2.1). *Inset table:* kinetic parameters based on the two curve fits. Changes in currents plateaued ~13 min after the application of PGE_2.

The following source data and figure supplements are available for figure 6:

Source data 1. Numerical data that were used to generate the chart in *Figure 6B*.
Source data 2. Numerical data that were used to generate the chart in *Figure 6C*.
Figure supplement 1. TRPV4 and Kir2.1 currents are preserved in cytoplasm-intact cECs.
Figure supplement 2. The muscarinic receptor agonist carbachol activates TRPV4 currents and inhibits Kir2.1 currents.
Figure supplement 3. Purinergic receptor activation affects Kir2.1 channels but not TRPV4 channels.

Discussion

We previously demonstrated that increases in $[K^+]_o$ associated with neuronal activity alter cerebral blood flow at the capillary level, showing that extracellular K^+ activates capillary Kir2.1 channels, triggering a retrograde electrical (hyperpolarizing) signal that propagates upstream to dilate feeding arterioles and enhance blood flow to the active region (*Longden et al., 2017*). We have also shown that G_qPCR-mediated PIP_2 depletion inhibits capillary electrical signaling (*Harraz et al., 2018*), identifying a point of intersection between electrical signaling and endothelial G_qPCR activity. In the present study, we show that cECs express TRPV4 channels, and demonstrate that these channels are tonically suppressed by basal levels of PIP_2. Furthermore, we show that G_qPCR activation relieves TRPV4 channel inhibition through PIP_2 depletion. This paradigm introduces the phosphoinositide PIP_2 as a master regulator of TRPV4 and Kir2.1 signaling in the capillary endothelium and highlights the ability of G_qPCR activity to tune the balance of these signaling modalities to favor TRPV4 signaling (*Figure 7*).

The repertoire of functional ion channels in brain cECs remains incompletely characterized, although certain molecular features have recently come into focus. For instance, our evidence suggests that the inward rectifier Kir2.1 channel is the major K^+ channel type in brain cECs (*Longden et al., 2017*), whereas Ca^{2+}-sensitive SK and IK channels, which are present in arterial and arteriolar ECs and play a prominent role in regulating vascular tone (*Ledoux et al., 2008*; *Sonkusare et al., 2012*; *Taylor et al., 2003*), are not expressed in brain cECs (*Longden et al., 2017*). Notably, the identity of depolarizing (Na^+ and/or Ca^{2+}-permeable) channels in cECs, which we predict must be present to allow the membrane potential to reset to support repeated operation of our previously reported Kir2.1-dependent electrical signaling-based NVC mechanism, is not known. Our demonstration that the highly selective TRPV4 agonist, GSK101, induced currents in brain cECs that were eliminated by the TRPV4-specific antagonist, HC-067047, and were absent in cECs from $TRPV4^{-/-}$ mice firmly establishes the presence of this non-selective cation channel in capillaries. In arterial and arteriolar ECs, TRPV4 channel-mediated Ca^{2+} influx is closely linked to activation of Ca^{2+}-sensitive SK and IK channels and subsequent membrane potential hyperpolarization (*Sonkusare et al., 2012*). However, because cECs lack functional Ca^{2+}-activated K^+ channels (*Longden et al., 2017*), TRPV4-mediated influx of Na^+/Ca^{2+} in these cells instead would lead to membrane potential depolarization (*Behringer et al., 2017*; *Earley and Brayden, 2015*). Collectively, these observations suggest that the TRPV4 channel is a major depolarizing element in cECs, although we cannot rule out the possibility that other, as yet unidentified, cation channels may contribute to membrane depolarization, as suggested by earlier studies (*Csanády and Adam-Vizi, 2004*; *Popp and Gögelein, 1992*; *Csanády and Adam-Vizi, 2003*). Our observations also highlight the fact that the functional role of TRPV4 channels is critically dependent on the expression and function of key associated proteins.
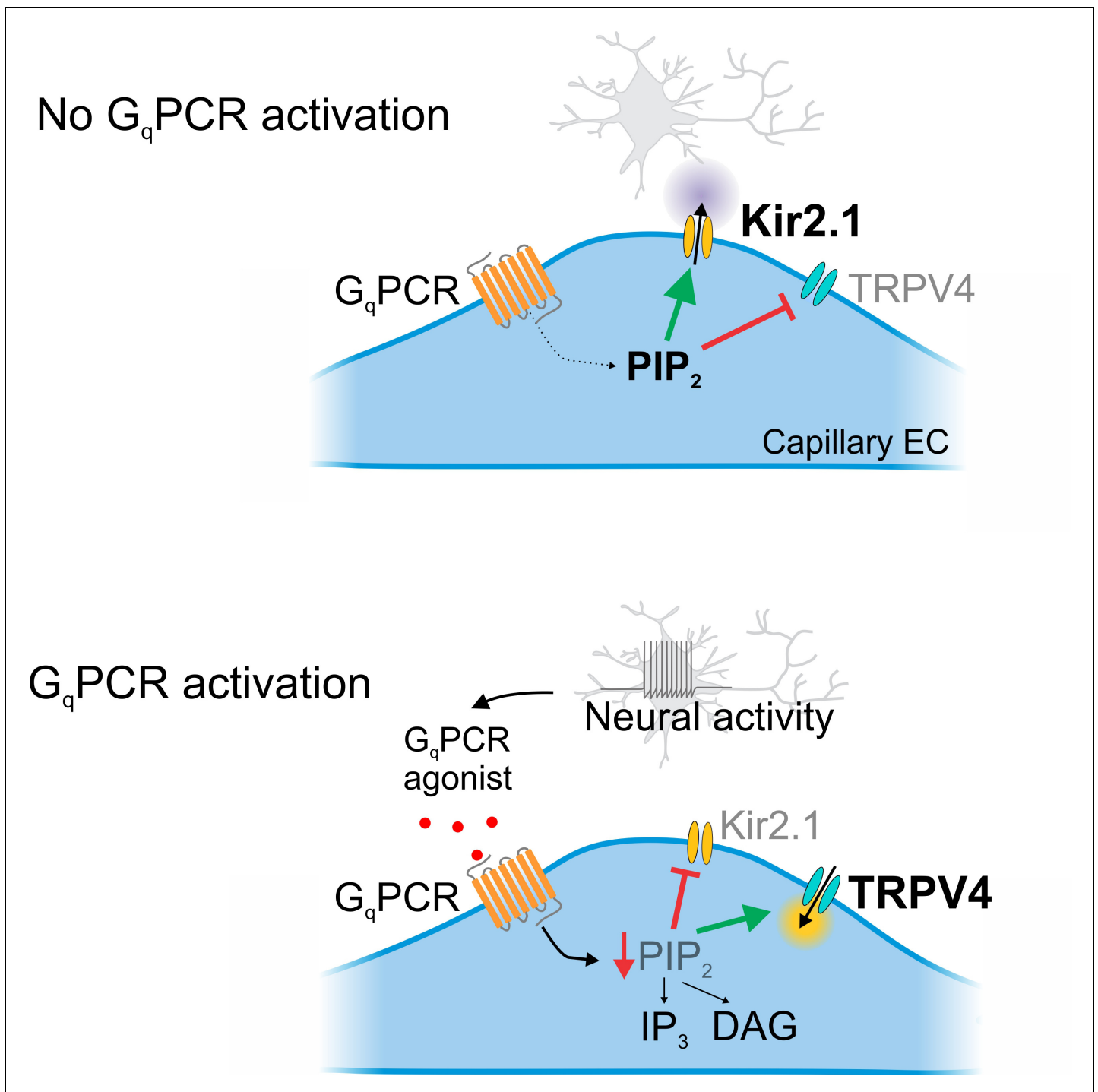
Figure 7. Cartoon representation of G_qPCR-mediated reciprocal effects on capillary ion channel activity. Schematic diagram summarizing the proposed mechanism. *Top*: In the absence of G_qPCR stimulation, endogenous PIP_2 levels are sufficient to tonically inhibit TRPV4 channels and maintain Kir2.1 channel activity. *Bottom*: G_qPCR activation with an agonist stimulates PIP_2 hydrolysis, resulting in the loss of PIP_2-mediated maintenance of Kir2.1 activity and inhibition of TRPV4 activity.

DOI: https://doi.org/10.7554/eLife.38689.033

Intriguingly, and in striking contrast to the case in peripheral arterial ECs (*Sonkusare et al., 2014*; *Sonkusare et al., 2012*), the open probability of capillary TRPV4 channels in cECs was remarkably low under basal conditions and was increased by dialyzing out intracellular contents—the first link in the chain leading to our discovery that TRPV4 channels in cECs are intrinsically inhibited by intracellular ATP. It is well established that lipid kinases involved in PIP_2 synthesis require millimolar ATP for their activity (*Balla and Balla, 2006*; *Hilgemann, 1997*; *Knight and Shokat, 2005*; *Suer et al., 2001*), and it has been amply demonstrated that PIP_2 maintenance is dependent on ATP in multiple cell types (*Suh and Hille, 2008*; *Ye et al., 2018*; *Zakharian et al., 2011*), including cECs (*Harraz et al., 2018*). Three major lines of evidence presented here support the conclusion that cytosolic ATP-dependent maintenance of sustained, basal levels of PIP_2 suppresses TRPV4 channel activity. First, millimolar concentrations of hydrolyzable ATP suppressed capillary TRPV4 channel activity. Second, inclusion of PIP_2 analogs in the patch pipette inhibited TRPV4 currents. Third, scavenging PIP_2 or inhibiting its synthesis abrogated ATP-mediated inhibition. Notably, PIP_2 has been reported to directly interact with different residues on the TRPV4 N-terminus in heterologous expression systems (*Garcia-Elias et al., 2013*; *Takahashi et al., 2014*). However, these studies reached discrepant conclusions, with one suggesting that direct binding of PIP_2 to the ankyrin repeat domain of the TRPV4 channel inhibits different modes of TRPV4 activation (*Takahashi et al., 2014*) and the other reporting that PIP_2 is necessary for heat-, hypotonicity- or epoxyeicosatrienoic acid (EET)-induced channel activation by facilitating structural rearrangements of the channel (*Garcia-Elias et al., 2013*). These discrepancies may reflect divergent effects of PIP_2 on channel behavior through binding to multiple sites in the channel. Intriguingly, the putative endogenous TRPV4 channel activator (*Earley and Brayden, 2015*; *Watanabe et al., 2003*) 11,12-epoxyeicosatrienoic acid (11,12-EET, 1 μM) evoked currents in cECs even in the absence of dialyzed PIP_2 (*Figure 3—figure supplement 2*). In any case, our results are the first to report PIP_2-mediated suppression of TRPV4 channels in the endothelium and more broadly in native cells and are congruent with the results of *Takahashi et al., 2014*. Interestingly, a recent study provided structural evidence that lipid molecules are tightly bound to the selectivity filter of the TRPV4 channel pore, although the identity and function of these lipids were not characterized (*Deng et al., 2018*).

Canonical G_qPCR signaling involves PLC activation and subsequent PIP_2 breakdown into DAG and IP_3. Receptor agonists that activate G_qPCRs can dramatically lower PIP_2 by promoting its hydrolysis at rates that exceed those of PIP_2 re-synthesis. We show here that PGE_2, which has previously been postulated to act as an NVC agent through actions on G_s-coupled EP_2/EP_4 receptors in arteriolar smooth muscle (*Lacroix et al., 2015*; *Zonta et al., 2003*), activates TRPV4 channels in cECs independent of the action of the PIP_2 metabolites, DAG and IP_3, by relieving PIP_2-mediated suppression (*Figure 4*, *Figure 5*). In contrast, we recently showed that G_qPCR agonists exert the opposite effect on capillary Kir2.1 channels, inhibiting their ability to mediate capillary-to-arteriole electrical signaling (*Harraz et al., 2018*). In keeping with these previous findings and our current observations, simultaneous monitoring of TRPV4 and Kir2.1 channel currents confirmed the bidirectional effects of G_qPCR agonists on the two channels (*Figure 6*). This two-way modulation (*Figure 7*) is unique as it indicates that a single G_qPCR signaling cascade is capable of altering the balance between electrical Kir2.1 signaling (*inhibition*) and TRPV4 signaling (*facilitation*). Given the absence of Ca^{2+}-activated K^+ channels in cECs, noted above, G_qPCR signaling-induced PIP_2 depletion would likely depolarize cECs through the simultaneous disinhibition of depolarizing TRPV4 channels (this study) and deactivation of hyperpolarizing Kir2.1 channels (*Harraz et al., 2018*).

Based on our direct Kir2.1 current measurements (*Harraz et al., 2018*; *Longden et al., 2017*) and the known voltage- and K^+-dependence of Kir2.1 channels (*Longden and Nelson, 2015*), we estimate that the outward current through these channels at physiological membrane potentials (about −40 mV) and external K^+ (3 mM) is ~6 fA. Elevation of external K^+ to 10 mM would increase Kir2 current at this voltage to ~260 fA. Though seemingly miniscule, such small membrane currents are precisely what is needed to ensure conduction fidelity. We have measured a sustained and profound hyperpolarization of about −25 mV in arteriolar smooth muscle in response to capillary stimulation with 10 mM K^+ (*Longden et al., 2017*). Our computational modeling indicates that a stable membrane hyperpolarization of 25 mV requires the outward (hyperpolarizing) current to greatly exceed the inward (depolarizing) current. Our estimate of basal, PIP_2-suppressed TRPV4 current at −40 mV is about −80 fA. G_qPCR activation increases open probability ~6 fold, producing a current (400–500 fA) sufficient to effectively short circuit K^+-induced hyperpolarization and cripple this key

Kir2.1-based NVC mechanism. In conclusion, the low level of TRPV4 channel activity aligns with the functional role of capillaries.

Activation of capillary G_qPCRs should also trigger Ca^{2+} signals in cECs, presumably through IP_3-mediated Ca^{2+} release from intracellular stores as well as disinhibition of TRPV4 channels (as described here) and subsequent Ca^{2+} influx. Such capillary Ca^{2+} signals should positively influence hemodynamics—and thus functional hyperemia—providing a plausible explanation for the role of G_qPCR agonists in the NVC process, presumably through the Ca^{2+}-dependent activation of nitric oxide synthase (NOS) and subsequent release of the vasodilator, NO (*Förstermann et al., 1991*; *Marziano et al., 2017*). Capillary Ca^{2+} signaling might also serve an entirely different purpose in functional hyperemia: because local Ca^{2+} signals represent sites of PIP_2 depletion (through G_qPCR signaling), and thus membrane potential depolarization (through TRPV4 disinhibition and Kir2.1 deactivation), they are likely to interfere with the progression of electrical signals generated further down the vascular tree. Accordingly, these signals may represent 'stop signs' or 'speed bumps' that play a role in redirecting hyperpolarizing (vasodilatory) signals away from certain brain areas, in addition to their role in resetting the capillary membrane potential, noted above.

Given the role of PIP_2 in negatively regulating TRPV4 channels, the exceedingly low basal TRPV4 activity and diminished sensitivity to GSK101 in cECs (*Figure 1*) compared with mesenteric artery ECs (*Sonkusare et al., 2012*) suggest differences in the PIP_2 'set point' in these two vascular beds. This supposition has important physiological implications for electrical signaling in the brain. Our data suggest that PIP_2 levels in brain cECs are sufficient to saturate Kir2.1 channels (*Harraz et al., 2018*) and tune TRPV4 channel currents to levels that prevent inappropriate depolarization of the membrane potential (*Figure 3*). In the absence of PIP_2 suppression of TRPV4 channel-mediated inward currents, it is unlikely that increased outward K^+ currents through Kir2.1 channels in response to elevated K^+ would be sufficient to cause membrane potential hyperpolarization. The mechanistic basis for the apparently higher PIP_2 set point in brain cECs is currently unknown, but could include lower constitutive G_qPCR activity, lower microenvironmental levels of G_qPCR agonists and/or decreased G_qPCR expression—and thus diminished PIP_2 breakdown. Along these lines, a recent single-cell transcriptomics analysis showed that $G\alpha_q$ (*Gnaq*) transcript levels in the mouse brain endothelium are reduced compared with those in peripheral pulmonary ECs (*Vanlandewijck et al., 2018*). Alternatively, differences in the set point could be indicative of more robust PIP_2 synthesis in brain capillaries, a speculation that is supported by the higher mitochondrial content—and hence ATP synthesis—in highly active brain cECs compared with other ECs (*Oldendorf and Brown, 1975*; *Oldendorf et al., 1977*).

In conclusion, this study provides compelling evidence that brain capillaries express TRPV4 channels and further shows that the activity of these channels is physiologically suppressed by basal levels of PIP_2. This introduces PIP_2 and its modulation by G_qPCR agonists as major regulators of brain capillary signaling. When maintained at sufficient levels, PIP_2 inhibits TRPV4 channels and supports capillary-to-arteriole electrical signaling, but in response to G_qPCR activation, PIP_2 levels are reduced, enhancing TRPV4 signaling and inhibiting retrograde electrical signaling via Kir2.1 channels. Capillary G_qPCRs can therefore be envisioned as molecular switches that dictate the signaling modality in the brain microvasculature.

Materials and methods

Key resources table

Reagent type (species) or resource	Designation	Source or reference	Identifiers	A
Strain, strain background (*Mus musculus*, males)	TRPV4 Knockout (TRPV4$^{-/-}$) mice, C57BL/6J background	*Thorneloe et al. (2008)*	PMID: 18499743	
Strain, strain background (*Mus musculus*, males)	C57BL/6J	The Jackson Laboratory	RRID:IMSR_JAX:000664	
Chemical compound, drug	GSK1016790A (GSK101)	Sigma	Cat#: G0798	

Continued on next page

Continued

Reagent type (species) or resource	Designation	Source or reference	Identifiers	A
Chemical compound, drug	Ruthenium red (RuR)	Sigma	Cat#: R2751	
Chemical compound, drug	Adenosine 5′-triphosphate magnesium salt (Mg-ATP)	Sigma	Cat#: A9187	
Chemical compound, drug	Adenosine 5′-triphosphate sodium salt	Sigma	Cat#: A2383	
Chemical compound, drug	HC-067047	Sigma	Cat#: SML0143	
Chemical compound, drug	KT5823	Sigma	Cat#: K1388	
Chemical compound, drug	PIK93	Tocris	Cat#: 6440	
Chemical compound, drug	Phenylarsine oxide (PAO)	Sigma	Cat# P3075	
Chemical compound, drug	H-89 dihydrochloride	Tocris	Cat# 2910	
Chemical compound, drug	Calphostin C	Tocris	Cat#: 1626	
Chemical compound, drug	LY294002 hydrochloride	Tocris	Cat#: 1130	
Chemical compound, drug	AH6809	Tocris	Cat#: 0671	
Chemical compound, drug	SC51322	Tocris	Cat#: 2791	
Chemical compound, drug	U-73122	Sigma	Cat#: U6756	
Chemical compound, drug	U-73343	Sigma	Cat#: U6881	
Chemical compound, drug	Poly-L-lysine hydrochloride	Sigma	Cat# 2658	
Chemical compound, drug	Gö6976	Calbiochem	Cat#: 365250	
Chemical compound, drug	Wortmannin	Sigma	Cat#: W1628	
Chemical compound, drug	PI(4,5)P2 (1,2-dioctanoyl) (sodium salt)	Cayman	Cat#: 64910	
Chemical compound, drug	PI(4,5)P2 (1,2-dipalmitoyl) (sodium salt)	Cayman	Cat#: 10008115	
Chemical compound, drug	Prostaglandin E_2	Sigma	Cat#: 5640	
Chemical compound, drug	SLIGRL-NH2	Tocris	Cat#: 1468	
Chemical compound, drug	Carbachol	Sigma	Cat#: C4382	
Chemical compound, drug	Cyclopiazonic acid from *Penicillium cyclopium* (CPA)	Sigma	Cat#: C1530	
Chemical compound, drug	Guanosine 5′-triphosphate sodium salt (GTP)	Sigma	Cat#: G8877	

Continued on next page

Continued

Reagent type (species) or resource	Designation	Source or reference	Identifiers	A
Chemical compound, drug	Adenosine 5′-[γ-thio]triphosphate tetralithium salt	Sigma	Cat#: A1388	
Chemical compound, drug	11,12-Epoxyeico satrienoic acid (11,12-EET)	Sigma	Cat#: E5641	
Chemical compound, drug	4α-Phorbol 12,13-didecanoate (4α-PDD)	Sigma	Cat#: P8014	
Chemical compound, drug	1,2-Bis (2-aminophenoxy) ethane-N,N,N′,N′-tetraacetic acid tetrapotassium salt (BAPTA)	Sigma	Cat#: A9801	
Software, algorithm	Prism	GraphPad	RRID:SCR_002798 https://www.graphpad.com/scientific-software/prism/	
Software, algorithm	Clampfit 10.7	Axon Instruments	RRID:SCR_011323 https://www.moleculardevices.com/products/axon-patch-clamp-system	

Animals

All procedures involving animals received prior approval from the University of Vermont Institutional Animal Care and Use Committee. Adult (2–3 month old) male C57BL/6J mice (Jackson Laboratories, USA) and TRPV4$^{-/-}$ mice (*Thorneloe et al., 2008*) were group-housed on a 12 hr light:dark cycle with environmental enrichment and free access to food and water. Animals were euthanized by intraperitoneal injection of sodium pentobarbital (100 mg/kg) followed by rapid decapitation.

Chemicals

1,2-Dioctanoyl phosphatidylinositol 4,5-bisphosphate sodium salt (diC8-PIP$_2$) and 1,2-dipalmitoyl phosphatidylinositol 4,5-bisphosphate sodium salt (diC16-PIP$_2$) were purchased from Cayman Chemical (USA). 12-(2-Cyanoethyl)−6,7,12,13-tetrahydro-13-methyl-5-oxo-5H-indolo(2,3-a)pyrrolo(3,4 c)-carbazole (Gö6976) was from Calbiochem (USA). N-((1S)−1-{[4-((2S)−2-{[(2,4-Dichlorophenyl) sulfonyl] amino}−3-hydroxy-propanoyl)−1-piperazinyl]carbonyl}−3-methylbutyl)−1-benzothiophene-2-carboxamide (GSK101) and 2-Methyl-1-[3-(4-morpholinyl)propyl]−5-phenyl-N-[3-(trifluoromethyl) phenyl]−1H–pyrrole-3-carboxamide (HC-067047) were obtained from Sigma-Aldrich (USA). 6-Isopropoxy-9-xanthone-2-carboxylic acid (AH6809), 8-chloro-2-[3-[(2-furanylmethyl)thio]−1-oxopropyl]-dibenz(Z)[b,f][1,4]oxazepine-10(11H)-carboxylic acid hydrazide (SC51322), N-[2-[[3-(4-bromophenyl)−2-propenyl]amino]ethyl]−5-isoquinolinesulfonamide dihydrochloride (H-89), (1R)−2-[12-[(2R)−2-(benzoyloxy)propyl]−3,10-dihydro-4,9-dihydroxy-2,6,7,11-tetramethoxy-3,10-dioxo-1-perylenyl]−1-methylethylcarbonic acid 4-hydroxyphenyl ester (calphostin C), and 2-(4-morpholinyl)−8-phenyl-4H-1-benzopyran-4-one hydrochloride (LY 294002) were purchased from Tocris (USA). Unless otherwise noted, all other chemicals were obtained from Sigma-Aldrich.

Capillary endothelial cell isolation

Single ECs and capillary fragments were obtained from mouse brains by mechanical disruption of two 160 µm–thick brain slices using a Dounce homogenizer. Slices were homogenized in ice-cold artificial cerebrospinal fluid (124 mM NaCl, 3 mM KCl, 2 mM CaCl$_2$, 2 mM MgCl$_2$, 1.25 mM NaH$_2$PO$_4$, 26 mM NaHCO$_3$, 4 mM glucose), and debris was removed by passing the homogenate through a 62 µm nylon mesh. Retained capillary fragments were eluted into dissociation solution composed of 55 mM NaCl, 80 mM Na-glutamate, 5.6 mM KCl, 2 mM MgCl$_2$, 4 mM glucose and 10 mM HEPES (pH 7.3), containing neutral protease (0.5 mg/mL) and elastase (0.5 mg/mL) (Worthington, USA) plus 100 µM CaCl$_2$, and incubated for 24 min at 37°C. Thereafter, 0.5 mg/ml collagenase type I (Worthington) was added and the sample was incubated for an additional 2 min at 37°C. The cell suspension was filtered and the residue was washed to remove enzymes. Single cells and small

capillary fragments were dispersed by triturating 4–6 times with a fire-polished glass Pasteur pipette. Cells were stored in ice-cold isolation medium for use the same day (within ~6 hr).

Electrophysiology

All patch-clamp electrophysiological recordings were performed at room temperature (~22°C) in either the conventional or perforated whole-cell configuration. Currents were amplified using an Axopatch 200B amplifier, filtered at 1 kHz, digitized at 10 kHz, and stored on a computer for offline analysis with Clampfit 10.5 software. Recording pipettes were fabricated by pulling borosilicate glass (1.5 mm outer diameter, 1.17 mm inner diameter; Sutter Instruments, USA) using a Narishige puller. Pipettes were fire-polished to reach a tip resistance of ~4–6 MΩ. The bath solution consisted of 80 or 134 mM NaCl, 60 or 6 mM KCl, 1 mM $MgCl_2$, 10 mM HEPES, 4 mM glucose, and 2 mM $CaCl_2$ (pH 7.4). For the conventional whole-cell configuration, pipettes were backfilled with a solution consisting of 10 mM NaOH, 11.4 mM KOH, 128.6 mM KCl, 1.1 mM $MgCl_2$, 2.2 mM $CaCl_2$, 5 mM EGTA, and 10 mM HEPES (pH 7.2). A subset of experiments utilized a Mg^{2+}-free solution, obtained by excluding $MgCl_2$ from the pipette solution. In another group of cells, EGTA was replaced with BAPTA (5.4 mM). For perforated-patch electrophysiology, the pipette solution was composed of 10 mM NaCl, 26.6 mM KCl, 110 mM K^+ aspartate, 1 mM $MgCl_2$ and 10 mM HEPES; amphotericin B (200–250 µg/ml) was freshly added on the day of the experiment. Whole-cell capacitance, measured using the cancellation circuitry in the voltage-clamp amplifier, averaged 8.6 pF.

Calculation of TRPV4 channel numbers

TRPV4 membrane currents were measured using the conventional whole-cell configuration and physiological concentrations of salts. Ruthenium red (RuR; 1 µM) was used to block Ca^{2+} influx and thereby prevent Ca^{2+} overload. We have shown previously that RuR causes a voltage-dependent block of TRPV channels and is rapidly driven out of the pore by membrane depolarization; at +100 mV, RuR (1 µM) blocks approximately 19% of the TRPV4 current (*Sonkusare et al., 2012*). The number of TRPV4 channels activated by 100 nM GSK101 was estimated by dividing the GSK101-induced current at +100 mV by the unitary current at this voltage (i.e. 10 pA) (*Loukin et al., 2010*; *Watanabe et al., 2002*) and correcting for the degree of RuR block.

Data analysis

Data are expressed as means ± standard error of the mean (SEM). Effects of a given condition/treatment on whole-cell current were compared using paired or unpaired *t* tests or analysis of variance (ANOVA), as appropriate, using Graphpad Prism 7.01 software. p values$\leq$0.05 were considered statistically significant. Additional patch-clamp data analyses were performed using Clampfit 10.5 software.

Acknowledgement

Additional information

Funding

Funder	Grant reference number	Author
American Heart Association	Postdoctoral fellowship 17POST33650030	Osama F Harraz
American Heart Association	Scientist Development Grant 17SDG33670237	Thomas A Longden

Author contributions

Osama F Harraz, Conceptualization, Data curation, Formal analysis, Funding acquisition, Investigation, Methodology, Writing—original draft, Writing—review and editing; Thomas A Longden, Funding acquisition, Investigation, Methodology, Writing—review and editing; David Hill-Eubanks, Writing—original draft, Writing—review and editing; Mark T Nelson, Conceptualization, Resources, Supervision, Funding acquisition, Writing—original draft, Writing—review and editing

Author ORCIDs

Osama F Harraz (iD) http://orcid.org/0000-0003-2061-1100
Mark T Nelson (iD) http://orcid.org/0000-0002-6608-8784

Ethics

Animal experimentation: This study was performed in strict accordance with the recommendations in the Guide for the Care and Use of Laboratory Animals of the National Institutes of Health. All procedures involving animals received prior approval from the University of Vermont Institutional Animal Care and Use Committee (IACUC, protocol # 14-063 and 16-010). Animals were euthanized by intraperitoneal injection of sodium pentobarbital (100 mg/kg) followed by rapid decapitation. Every effort was made to minimize suffering of animal subjects.

Decision letter and Author response

Decision letter https://doi.org/10.7554/eLife.38689.040
Author response https://doi.org/10.7554/eLife.38689.041

Additional files

Supplementary files

• Transparent reporting form
DOI: https://doi.org/10.7554/eLife.38689.034

Data availability

All data generated or analyzed during this study are included in the manuscript and supporting source data files.

The following previously published datasets were used:

Author(s)	Year	Dataset title	Dataset URL	Database, license, and accessibility information
Vanlandewijck M, He L, Mäe M, Andrae J, Betsholtz C	2017	Single cell RNA-seq of mouse brain vascular transcriptomes	https://www.ncbi.nlm.nih.gov/geo/query/acc.cgi?acc=GSE98816	Publicly available at the NCBI Gene Expression Omnibus (accession no. GSE98816)
Vanlandewijck M, He L, Mäe M, Andrae J, Betsholtz C	2017	Single cell RNA-seq of mouse lung vascular transcriptomes	https://www.ncbi.nlm.nih.gov/geo/query/acc.cgi?acc=GSE99235	Publicly available at the NCBI Gene Expression Omnibus (accession no. GSE99235)

References

Balla A, Balla T. 2006. Phosphatidylinositol 4-kinases: old enzymes with emerging functions. *Trends in Cell Biology* **16**:351–361. DOI: https://doi.org/10.1016/j.tcb.2006.05.003, PMID: 16793271

Baukrowitz T, Schulte U, Oliver D, Herlitze S, Krauter T, Tucker SJ, Ruppersberg JP, Fakler B. 1998. PIP_2 and PIP as determinants for ATP inhibition of K_{ATP} channels. *Science* **282**:1141–1144. DOI: https://doi.org/10.1126/science.282.5391.1141, PMID: 9804555

Behringer EJ, Scallan JP, Jafarnejad M, Castorena-Gonzalez JA, Zawieja SD, Moore JE, Davis MJ, Segal SS. 2017. Calcium and electrical dynamics in lymphatic endothelium. *The Journal of Physiology* **595**:7347–7368. DOI: https://doi.org/10.1113/JP274842, PMID: 28994159

Blinder P, Tsai PS, Kaufhold JP, Knutsen PM, Suhl H, Kleinfeld D. 2013. The cortical angiome: an interconnected vascular network with noncolumnar patterns of blood flow. *Nature Neuroscience* **16**:889–897. DOI: https://doi.org/10.1038/nn.3426, PMID: 23749145

Cho H, Kim YA, Yoon JY, Lee D, Kim JH, Lee SH, Ho WK. 2005a. Low mobility of phosphatidylinositol 4,5-bisphosphate underlies receptor specificity of Gq-mediated ion channel regulation in atrial myocytes. *PNAS* **102**:15241–15246. DOI: https://doi.org/10.1073/pnas.0408851102, PMID: 16217031

Cho H, Lee D, Lee SH, Ho WK. 2005b. Receptor-induced depletion of phosphatidylinositol 4,5-bisphosphate inhibits inwardly rectifying K^+ channels in a receptor-specific manner. *PNAS* **102**:4643–4648. DOI: https://doi.org/10.1073/pnas.0408844102, PMID: 15767570

Csanády L, Adam-Vizi V. 2003. Ca^{2+}- and voltage-dependent gating of Ca^{2+}- and ATP-sensitive cationic channels in brain capillary endothelium. *Biophysical Journal* **85**:313–327. DOI: https://doi.org/10.1016/S0006-3495(03)74476-2, PMID: 12829486

Csanády L, Adam-Vizi V. 2004. Antagonistic regulation of native Ca^{2+}- and ATP-sensitive cation channels in brain capillaries by nucleotides and decavanadate. *The Journal of General Physiology* **123**:743–757. DOI: https://doi.org/10.1085/jgp.200309008, PMID: 15173222

D'Avanzo N, Cheng WW, Doyle DA, Nichols CG. 2010. Direct and specific activation of human inward rectifier K^+ channels by membrane phosphatidylinositol 4,5-bisphosphate. *Journal of Biological Chemistry* **285**:37129–37132. DOI: https://doi.org/10.1074/jbc.C110.186692, PMID: 20921230

Deng Z, Paknejad N, Maksaev G, Sala-Rabanal M, Nichols CG, Hite RK, Yuan P. 2018. Cryo-EM and X-ray structures of TRPV4 reveal insight into ion permeation and gating mechanisms. *Nature Structural & Molecular Biology* **25**:252–260. DOI: https://doi.org/10.1038/s41594-018-0037-5, PMID: 29483651

Dickson EJ, Falkenburger BH, Hille B. 2013. Quantitative properties and receptor reserve of the IP_3 and calcium branch of G_q-coupled receptor signaling. *The Journal of General Physiology* **141**:521–535. DOI: https://doi.org/10.1085/jgp.201210886, PMID: 23630337

Earley S, Brayden JE. 2015. Transient receptor potential channels in the vasculature. *Physiological Reviews* **95**:645–690. DOI: https://doi.org/10.1152/physrev.00026.2014, PMID: 25834234

Förstermann U, Pollock JS, Schmidt HH, Heller M, Murad F. 1991. Calmodulin-dependent endothelium-derived relaxing factor/nitric oxide synthase activity is present in the particulate and cytosolic fractions of bovine aortic endothelial cells. *PNAS* **88**:1788–1792. DOI: https://doi.org/10.1073/pnas.88.5.1788, PMID: 1705708

Garcia-Elias A, Mrkonjic S, Pardo-Pastor C, Inada H, Hellmich UA, Rubio-Moscardó F, Plata C, Gaudet R, Vicente R, Valverde MA. 2013. Phosphatidylinositol-4,5-biphosphate-dependent rearrangement of TRPV4 cytosolic tails enables channel activation by physiological stimuli. *PNAS* **110**:9553–9558. DOI: https://doi.org/10.1073/pnas.1220231110, PMID: 23690576

Hansen SB, Tao X, MacKinnon R. 2011. Structural basis of PIP_2 activation of the classical inward rectifier K^+ channel Kir2.2. *Nature* **477**:495–498. DOI: https://doi.org/10.1038/nature10370, PMID: 21874019

Harraz OF, Longden TA, Dabertrand F, Hill-Eubanks D, Nelson MT. 2018. Endothelial GqPCR activity controls capillary electrical signaling and brain blood flow through PIP_2 depletion. *PNAS* **115**:E3569–E3577. DOI: https://doi.org/10.1073/pnas.1800201115, PMID: 29581272

Hibino H, Inanobe A, Furutani K, Murakami S, Findlay I, Kurachi Y. 2010. Inwardly rectifying potassium channels: their structure, function, and physiological roles. *Physiological Reviews* **90**:291–366. DOI: https://doi.org/10.1152/physrev.00021.2009, PMID: 20086079

Hilgemann DW. 1997. Cytoplasmic ATP-dependent regulation of ion transporters and channels: mechanisms and messengers. *Annual Review of Physiology* **59**:193–220. DOI: https://doi.org/10.1146/annurev.physiol.59.1.193, PMID: 9074761

Hille B, Dickson EJ, Kruse M, Vivas O, Suh B-C. 2015. Phosphoinositides regulate ion channels. *Biochimica Et Biophysica Acta (BBA) - Molecular and Cell Biology of Lipids* **1851**:844–856. DOI: https://doi.org/10.1016/j.bbalip.2014.09.010

Huang CL, Feng S, Hilgemann DW. 1998. Direct activation of inward rectifier potassium channels by PIP_2 and its stabilization by Gβγ. *Nature* **391**:803–806. DOI: https://doi.org/10.1038/35882, PMID: 9486652

Iadecola C, Nedergaard M. 2007. Glial regulation of the cerebral microvasculature. *Nature Neuroscience* **10**: 1369–1376. DOI: https://doi.org/10.1038/nn2003, PMID: 17965657

Jung SR, Seo JB, Deng Y, Asbury CL, Hille B, Koh DS. 2016. Contributions of protein kinases and β-arrestin to termination of protease-activated receptor 2 signaling. *The Journal of General Physiology* **147**:255–271. DOI: https://doi.org/10.1085/jgp.201511477, PMID: 26927499

Knight ZA, Shokat KM. 2005. Features of selective kinase inhibitors. *Chemistry & Biology* **12**:621–637. DOI: https://doi.org/10.1016/j.chembiol.2005.04.011, PMID: 15975507

Lacroix A, Toussay X, Anenberg E, Lecrux C, Ferreirós N, Karagiannis A, Plaisier F, Chausson P, Jarlier F, Burgess SA, Hillman EM, Tegeder I, Murphy TH, Hamel E, Cauli B. 2015. COX-2-Derived prostaglandin E2 produced by pyramidal neurons contributes to neurovascular coupling in the rodent cerebral cortex. *Journal of Neuroscience* **35**:11791–11810. DOI: https://doi.org/10.1523/JNEUROSCI.0651-15.2015, PMID: 26311764

Ledoux J, Taylor MS, Bonev AD, Hannah RM, Solodushko V, Shui B, Tallini Y, Kotlikoff MI, Nelson MT. 2008. Functional architecture of inositol 1,4,5-trisphosphate signaling in restricted spaces of myoendothelial projections. *PNAS* **105**:9627–9632. DOI: https://doi.org/10.1073/pnas.0801963105, PMID: 18621682

Longden TA, Dabertrand F, Koide M, Gonzales AL, Tykocki NR, Brayden JE, Hill-Eubanks D, Nelson MT. 2017. Capillary K^+-sensing initiates retrograde hyperpolarization to increase local cerebral blood flow. *Nature Neuroscience* **20**:717–726. DOI: https://doi.org/10.1038/nn.4533, PMID: 28319610

Longden TA, Nelson MT. 2015. Vascular inward rectifier K^+ channels as external K^+ sensors in the control of cerebral blood flow. *Microcirculation* **22**:183–196. DOI: https://doi.org/10.1111/micc.12190, PMID: 25641345

Loukin S, Zhou X, Su Z, Saimi Y, Kung C. 2010. Wild-type and brachyolmia-causing mutant TRPV4 channels respond directly to stretch force. *Journal of Biological Chemistry* **285**:27176–27181. DOI: https://doi.org/10.1074/jbc.M110.143370, PMID: 20605796

Marziano C, Hong K, Cope EL, Kotlikoff MI, Isakson BE, Sonkusare SK. 2017. Nitric Oxide-Dependent feedback loop regulates transient receptor potential vanilloid 4 (TRPV4) Channel cooperativity and endothelial function in small pulmonary arteries. *Journal of the American Heart Association* **6**:e007157. DOI: https://doi.org/10.1161/JAHA.117.007157, PMID: 29275372

Nilius B, Owsianik G, Voets T. 2008. Transient receptor potential channels meet phosphoinositides. *The EMBO Journal* **27**:2809–2816. DOI: https://doi.org/10.1038/emboj.2008.217, PMID: 18923420

O'Rourke B. 1993. Ion channels as sensors of cellular energy. mechanisms for modulation by magnesium and nucleotides. *Biochemical Pharmacology* **46**:1103–1112. DOI: https://doi.org/10.1016/0006-2952(93)90456-7, PMID: 7692854

Oldendorf WH, Brown WJ. 1975. Greater number of capillary endothelial cell mitochondria in brain than in muscle. *Experimental Biology and Medicine* **149**:736–738. DOI: https://doi.org/10.3181/00379727-149-38889

Oldendorf WH, Cornford ME, Brown WJ. 1977. The large apparent work capability of the blood-brain barrier: a study of the mitochondrial content of capillary endothelial cells in brain and other tissues of the rat. *Annals of Neurology* **1**:409–417. DOI: https://doi.org/10.1002/ana.410010502, PMID: 617259

Popp R, Gögelein H. 1992. A calcium and ATP sensitive nonselective cation channel in the antiluminal membrane of rat cerebral capillary endothelial cells. *Biochimica Et Biophysica Acta (BBA) - Biomembranes* **1108**:59–66. DOI: https://doi.org/10.1016/0005-2736(92)90114-2

Raichle ME, Mintun MA. 2006. Brain work and brain imaging. *Annual Review of Neuroscience* **29**:449–476. DOI: https://doi.org/10.1146/annurev.neuro.29.051605.112819, PMID: 16776593

Rohacs T. 2009. Phosphoinositide regulation of non-canonical transient receptor potential channels. *Cell Calcium* **45**:554–565. DOI: https://doi.org/10.1016/j.ceca.2009.03.011, PMID: 19376575

Ryves WJ, Harwood AJ. 2001. Lithium inhibits glycogen synthase kinase-3 by competition for magnesium. *Biochemical and Biophysical Research Communications* **280**:720–725. DOI: https://doi.org/10.1006/bbrc.2000.4169, PMID: 11162580

Sonkusare SK, Bonev AD, Ledoux J, Liedtke W, Kotlikoff MI, Heppner TJ, Hill-Eubanks DC, Nelson MT. 2012. Elementary Ca^{2+} signals through endothelial TRPV4 channels regulate vascular function. *Science* **336**:597–601. DOI: https://doi.org/10.1126/science.1216283, PMID: 22556255

Sonkusare SK, Dalsgaard T, Bonev AD, Hill-Eubanks DC, Kotlikoff MI, Scott JD, Santana LF, Nelson MT. 2014. AKAP150-dependent cooperative TRPV4 channel gating is central to endothelium-dependent vasodilation and is disrupted in hypertension. *Science Signaling* **7**:ra66. DOI: https://doi.org/10.1126/scisignal.2005052, PMID: 25005230

Sromek SM, Harden TK. 1998. Agonist-induced internalization of the $P2Y_2$ receptor. *Molecular Pharmacology* **54**:485–494. DOI: https://doi.org/10.1124/mol.54.3.485, PMID: 9730907

Suer S, Sickmann A, Meyer HE, Herberg FW, Heilmeyer LM. 2001. Human phosphatidylinositol 4-kinase isoform PI4K92. expression of the recombinant enzyme and determination of multiple phosphorylation sites. *European Journal of Biochemistry* **268**:2099–2106. DOI: https://doi.org/10.1046/j.1432-1327.2001.02089.x, PMID: 11277933

Suh BC, Hille B. 2002. Recovery from muscarinic modulation of M current channels requires phosphatidylinositol 4,5-bisphosphate synthesis. *Neuron* **35**:507–520. DOI: https://doi.org/10.1016/S0896-6273(02)00790-0, PMID: 12165472

Suh BC, Hille B. 2008. PIP2 is a necessary cofactor for ion channel function: how and why? *Annual Review of Biophysics* **37**:175–195. DOI: https://doi.org/10.1146/annurev.biophys.37.032807.125859, PMID: 18573078

Takahashi N, Hamada-Nakahara S, Itoh Y, Takemura K, Shimada A, Ueda Y, Kitamata M, Matsuoka R, Hanawa-Suetsugu K, Senju Y, Mori MX, Kiyonaka S, Kohda D, Kitao A, Mori Y, Suetsugu S. 2014. TRPV4 channel activity is modulated by direct interaction of the ankyrin domain to PI(4,5)P$_2$. *Nature Communications* **5**:4994. DOI: https://doi.org/10.1038/ncomms5994, PMID: 25256292

Taylor MS, Bonev AD, Gross TP, Eckman DM, Brayden JE, Bond CT, Adelman JP, Nelson MT. 2003. Altered expression of small-conductance Ca^{2+}-activated K$^+$ (SK3) channels modulates arterial tone and blood pressure. *Circulation Research* **93**:124–131. DOI: https://doi.org/10.1161/01.RES.0000081980.63146.69, PMID: 12805243

Thorneloe KS, Sulpizio AC, Lin Z, Figueroa DJ, Clouse AK, McCafferty GP, Chendrimada TP, Lashinger ES, Gordon E, Evans L, Misajet BA, Demarini DJ, Nation JH, Casillas LN, Marquis RW, Votta BJ, Sheardown SA, Xu X, Brooks DP, Laping NJ, et al. 2008. N-((1S)-1-{[4-((2S)-2-{[(2,4-dichlorophenyl)sulfonyl]amino}-3-hydroxypropanoyl)-1-piperazinyl]carbonyl}-3-methylbutyl)-1-benzothiophene-2-carboxamide (GSK1016790A), a novel and potent transient receptor potential vanilloid 4 channel agonist induces urinary bladder contraction and hyperactivity: Part I. *Journal of Pharmacology and Experimental Therapeutics* **326**:432–442. DOI: https://doi.org/10.1124/jpet.108.139295, PMID: 18499743

Vanlandewijck M, He L, Mäe MA, Andrae J, Ando K, Del Gaudio F, Nahar K, Lebouvier T, Laviña B, Gouveia L, Sun Y, Raschperger E, Räsänen M, Zarb Y, Mochizuki N, Keller A, Lendahl U, Betsholtz C. 2018. A molecular atlas of cell types and zonation in the brain vasculature. *Nature* **554**:475–480. DOI: https://doi.org/10.1038/nature25739, PMID: 29443965

Watanabe H, Vriens J, Suh SH, Benham CD, Droogmans G, Nilius B. 2002. Heat-evoked activation of TRPV4 channels in a HEK293 cell expression system and in native mouse aorta endothelial cells. *Journal of Biological Chemistry* **277**:47044–47051. DOI: https://doi.org/10.1074/jbc.M208277200, PMID: 12354759

Watanabe H, Vriens J, Prenen J, Droogmans G, Voets T, Nilius B. 2003. Anandamide and arachidonic acid use epoxyeicosatrienoic acids to activate TRPV4 channels. *Nature* **424**:434–438. DOI: https://doi.org/10.1038/nature01807, PMID: 12879072

White JP, Cibelli M, Urban L, Nilius B, McGeown JG, Nagy I. 2016. TRPV4: molecular conductor of a diverse orchestra. *Physiological Reviews* **96**:911–973. DOI: https://doi.org/10.1152/physrev.00016.2015, PMID: 27252279

Xie LH, Takano M, Kakei M, Okamura M, Noma A. 1999. Wortmannin, an inhibitor of phosphatidylinositol kinases, blocks the MgATP-dependent recovery of Kir6.2/SUR2A channels. *The Journal of Physiology* **514**:655–665. DOI: https://doi.org/10.1111/j.1469-7793.1999.655ad.x, PMID: 9882737

Ye W, Han TW, Nassar LM, Zubia M, Jan YN, Jan LY. 2018. Phosphatidylinositol-(4, 5)-bisphosphate regulates calcium gating of small-conductance cation channel TMEM16F. *PNAS* **115**:E1667–E1674. DOI: https://doi.org/10.1073/pnas.1718728115, PMID: 29382763

Zakharian E, Cao C, Rohacs T. 2011. Intracellular ATP supports TRPV6 activity *via* lipid kinases and the generation of PtdIns(4,5)P$_2$. *FASEB Journal: Official Publication of the Federation of American Societies for Experimental Biology* **25**:3915–3928. DOI: https://doi.org/10.1096/fj.11-184630, PMID: 21810903

Zonta M, Angulo MC, Gobbo S, Rosengarten B, Hossmann KA, Pozzan T, Carmignoto G. 2003. Neuron-to-astrocyte signaling is central to the dynamic control of brain microcirculation. *Nature Neuroscience* **6**:43–50. DOI: https://doi.org/10.1038/nn980, PMID: 12469126